ELEMENTA
Science of the Anthropocene

Haddon, A, et al. 2025. Simulated increases of future Arctic dimethylsulfide ocean concentrations, emissions and high-flux events. *Elem Sci Anth*, 13: 1. DOI: https://doi.org/10.1525/elementa.2024.00090

RESEARCH ARTICLE

Simulated increases of future Arctic dimethylsulfide ocean concentrations, emissions and high-flux events

Antoine Haddon[1,*], Adam H. Monahan[1], Tessa Sou[2], and Nadja Steiner[1,2,3]

Simulations from a regional ocean and sea ice model are presented to analyze the potential impacts of climate change on dimethylsulfide (DMS) ocean concentrations and emissions in the Arctic Ocean during the 21st century for a scenario of strong warming (RCP8.5, 2016–2085). The model used includes sulfur biogeochemistry in both the ocean and sea ice, representing the production of dimethylsulfoniopropionate and its conversion to DMS. Simulated DMS concentrations and emissions increase overall in the future throughout the Arctic. Substantial increases of summer ocean surface DMS concentrations and emissions are projected in the shallow continental shelves of the Eastern Arctic, due to a large reduction of sea ice cover. In the Central and Western Arctic, moderate increases of spring DMS production are trapped below sea ice even in the late 21st century. In deep basins, despite ice-free summers in the future, simulated DMS emissions are low, as DMS production occurs mostly below the mixed layer and remains at depth. The strong temporal variability of near-surface winds results in bursts of DMS emissions lasting a few days, with sea-to-air fluxes up to 10 times higher than the monthly median emissions rate. These spikes of DMS emissions occur throughout the Arctic, indicating an episodic impact of DMS on climate in areas of low mean DMS emissions. The simulated frequency of high-flux events increases during the 21st century in both spring and summer in almost all regions of the Arctic. However, the model is not capable of representing rapid out-gassing events during sea ice break-up, and improvements in the representation of leads are still necessary to fully assess the role of sea ice DMS production. With the ongoing decrease in anthropogenic sulfur emissions, these results suggest a future amplification of the role of DMS in aerosol and cloud formation in the Arctic.

Keywords: Dimethylsulfide, Sulfur, Arctic, Biogeochemistry, Future

1. Introduction

The impact of natural and anthropogenic aerosols on cloud dynamics and radiative forcing remains one of the largest uncertainties in projections of climate change (IPCC, 2021). In the Arctic, background particle concentrations are low, especially during summer when the polar front retreats northward, isolating the atmosphere from aerosols emitted from continental land masses. As a result, at high latitudes, natural aerosols such as sulfate aerosols play an active role in climate as a source of cloud condensation nuclei (CCN) or by directly scattering light back to space (Andreae and Raemdonck, 1983; Bates et al., 1992; Abbatt et al., 2019). Dimethylsulfide (DMS) is the most abundant source of naturally occurring sulfate aerosol particles in remote marine environments, and recent observations have shown that DMS actively contributes to the growth of particles to climate-relevant size and their subsequent activation as CCN (Park et al., 2017; 2021).

DMS originates in the ocean from the degradation of dimethylsulfoniopropionate (DMSP), which in turn is produced by phytoplankton, with varying production capacities among different groups of primary producers (Bullock et al., 2017). Phytoplankton and ice algae with high DMSP production capacities are abundant at high latitudes, increasing the relevance of sulfur biogeochemistry to Arctic climate (Levasseur, 2013). The role of microalgae as producers of a precursor to a climate-active gas is a source of potential interactions between ocean biogeochemistry and the climate. Understanding the oceanic sources of sulfate aerosols is therefore important to simulate the present and future climate and to further our understanding of interactions between the ocean, sea ice and the atmosphere.

DMS production and emissions have been included in ocean and sea ice models, starting with conceptual and 1D models (Jodwalis et al., 2000; Gabric et al., 2001). The first studies using global climate models explored the future of

[1] School of Earth and Ocean Sciences, University of Victoria, Victoria, BC, Canada
[2] Fisheries and Oceans Canada, Institute of Ocean Sciences, Sidney, BC, Canada
[3] Canadian Center for Climate Modelling and Analysis, Environment and Climate Change Canada, Victoria, BC, Canada
* Corresponding author:
Email: ahaddon@uvic.ca

DMS and found contrasting results, with both increases and decreases of global DMS emissions and concentrations simulated during the 21st century (Gabric et al., 2005; Kloster et al., 2007). For the Arctic, however, the models that include ocean sulfur biogeochemistry, participating in the Coupled Model Intercomparison Project phase 6 (CMIP6), project an increase of DMS emissions (Bock et al., 2021). This trend has been attributed mainly to the reduction in sea ice cover, as sea ice loss corresponds to the removal of a physical barrier to emissions. Recent increases of DMS emissions in the Arctic have been estimated from satellite-based observations (Galí et al., 2019), and atmospheric sampling campaigns have found increases of DMS oxidation products over the last two decades (Moffett et al., 2020). The future of DMS production in the Arctic remains uncertain, and CMIP6 model projections disagree on future trends of ocean surface DMS concentrations, with uncertainty linked to the future of primary production (Bock et al., 2021). Sea ice loss and the associated greater light availability are expected to increase the growth of phytoplankton in areas of historically low DMS and primary productivity. However, this effect could be offset by increasing stratification, resulting in greater nutrient limitation in the upper ocean and sea ice (Vancoppenolle et al., 2013; Timmermans and Marshall, 2020). Furthermore, climate change could affect phytoplankton and bacterial community composition, which will alter DMSP and DMS production in the Arctic (Campen et al., 2022).

In this work, we used a regional ocean and sea ice model with representations of the pelagic and sympagic ecosystems to simulate future Arctic DMS production and emissions, in order to understand how sulfur biogeochemistry will be impacted by climate change. For reasons of computational cost, we considered a single simulation forced with a single realization of the driving atmospheric variability, so we cannot quantify uncertainty associated with internal variability and model differences. As such, the focus of this study is a qualitative understanding of the mechanisms controlling DMS emissions and concentrations in the context of future climate change, and how physical and biological drivers can affect model projections.

Simulations of the model used here for the historical period (1979–2015) have been analyzed previously, showing good agreement with available DMS data and reproducing the observed increasing trend of DMS emissions (Hayashida et al., 2020). Here, we analyzed how DMS emissions will change in response to altered physical drivers, with a focus on understanding how sea ice cover and wind speed produce spatial and temporal variability. We also studied future DMS concentrations, with the particularity that in contrast to CMIP6 models we included a representation of sea ice sulfur biogeochemistry. Sensitivity tests with the model we used have indicated that DMS production in sea ice can be the main source of DMS emissions, especially at higher latitudes during spring (Hayashida et al., 2020). With the sea ice loss projected in the 21st century under scenarios of strong warming, sea ice DMS production will undoubtedly undergo large changes, which we explored here. Furthermore, we studied the relationship between DMS and primary production and how it results in changes in temporal and spatial variability of ocean DMS concentrations. As the physical dynamics of the Arctic Ocean are also impacted by climate change, we analyzed how altered stratification can affect ocean DMS concentrations and their vertical distribution in the water column.

2. Methods

2.1. Model

We present simulations from a regional model of the Arctic Ocean based on the physical ocean model NEMO 3.4 (Madec et al., 2017) and the sea ice model LIM2 (Bouillon et al., 2009). The model includes pelagic and sympagic biogeochemical components. Pelagic biogeochemical processes are represented by the Canadian Ocean Ecosystem Model (CanOE; Christian et al., 2022), which considers two primary producers and two zooplankton groups, as well as carbon and nitrogen chemistry. In sea ice, the Canadian Sea Ice Biogeochemistry model (CSIB; Mortenson et al., 2017; Hayashida et al., 2019) simulates a three-variable sea-ice ecosystem (ice algae, nitrate, and ammonium), as well as sulfur and carbon biochemistry, and is coupled to the pelagic biogeochemical model through exchanges at the sea ice–ocean interface. **Figure 2** from Hayashida et al. (2019) presents how the different elements of the model are connected and interact.

The model domain is based on the North Atlantic and Arctic (NAA) configuration, developed by the ocean modeling group at the University of Alberta (Hu and Myers, 2013), and was built on the curvilinear orthogonal coordinate system used by the NEMO model. The spatial domain (**Figure 1**) covers the entire Arctic north of approximately 60°N, the Bering Strait and the northern North Atlantic, with a horizontal resolution ranging from 10 km to 14.5 km and with 46 vertical ocean layers. For the present analysis, the Arctic was divided into 10 regions, based on the regions proposed by Matrai and Apollonio (2013), and which have been used in previous studies of future Arctic climate projections (Reader and Steiner, 2022; Steiner and Reader, 2024).

2.1.1. Sulfur biogeochemistry

The sulfur biogeochemistry component (**Figure 2**) was first developed in the context of a single column model (Hayashida et al., 2017) and subsequently integrated into the 3D configuration used here (Hayashida et al., 2019). We considered the configuration evaluated in Hayashida et al. (2020), in which a simulation over the historical period (1979–2015) was compared to available observations.

In sea ice and the ocean, the model represents DMSP in both particulate (DMSPp) and dissolved (DMSPd) forms, as well as DMS. The concentration of DMSPp is assumed to be proportional to carbon biomass of the primary producers, with different DMSP-to-carbon ratios for each group. In this model, the release of DMSPp from algal cells and its transformation into DMSPd occur through cell lysis, exudation, and sloppy feeding. DMSPd is then converted into DMS by bacteria and free DMSP-lyase enzymes, and DMS is

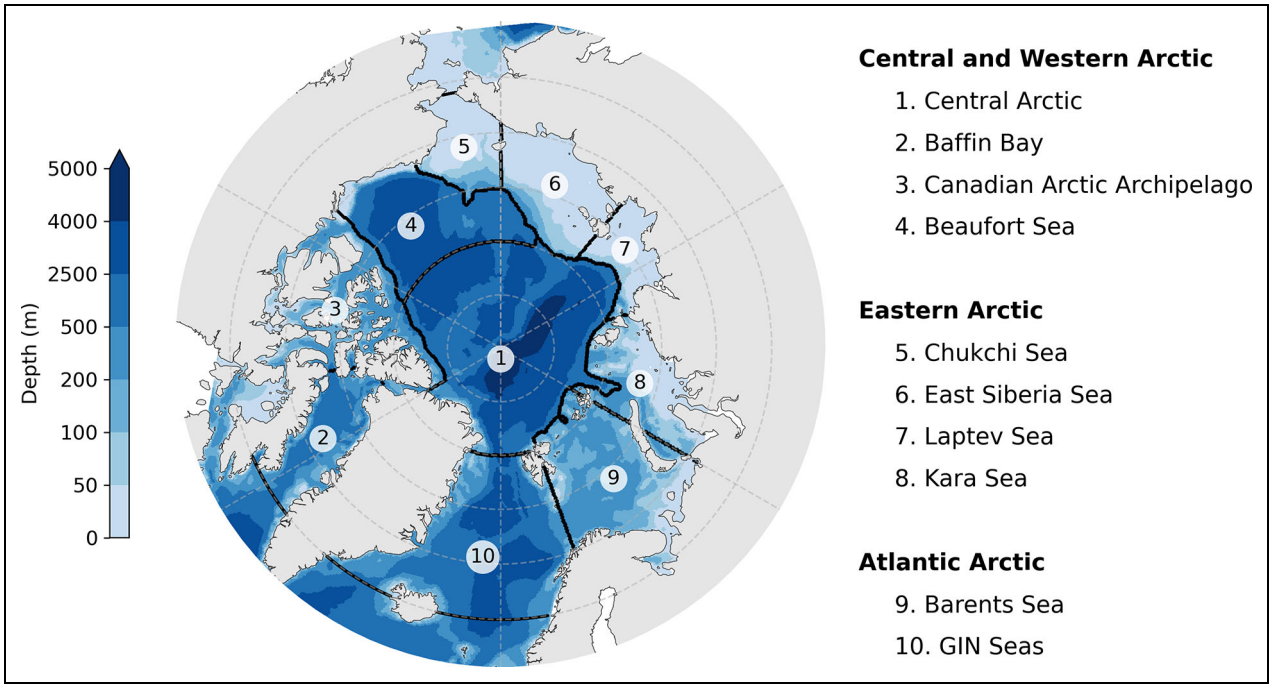

Figure 1. Map of the Arctic depicting regions used in the analysis of model simulations. Regional groups are in bold. GIN indicates Greenland, Iceland, and Norwegian seas.

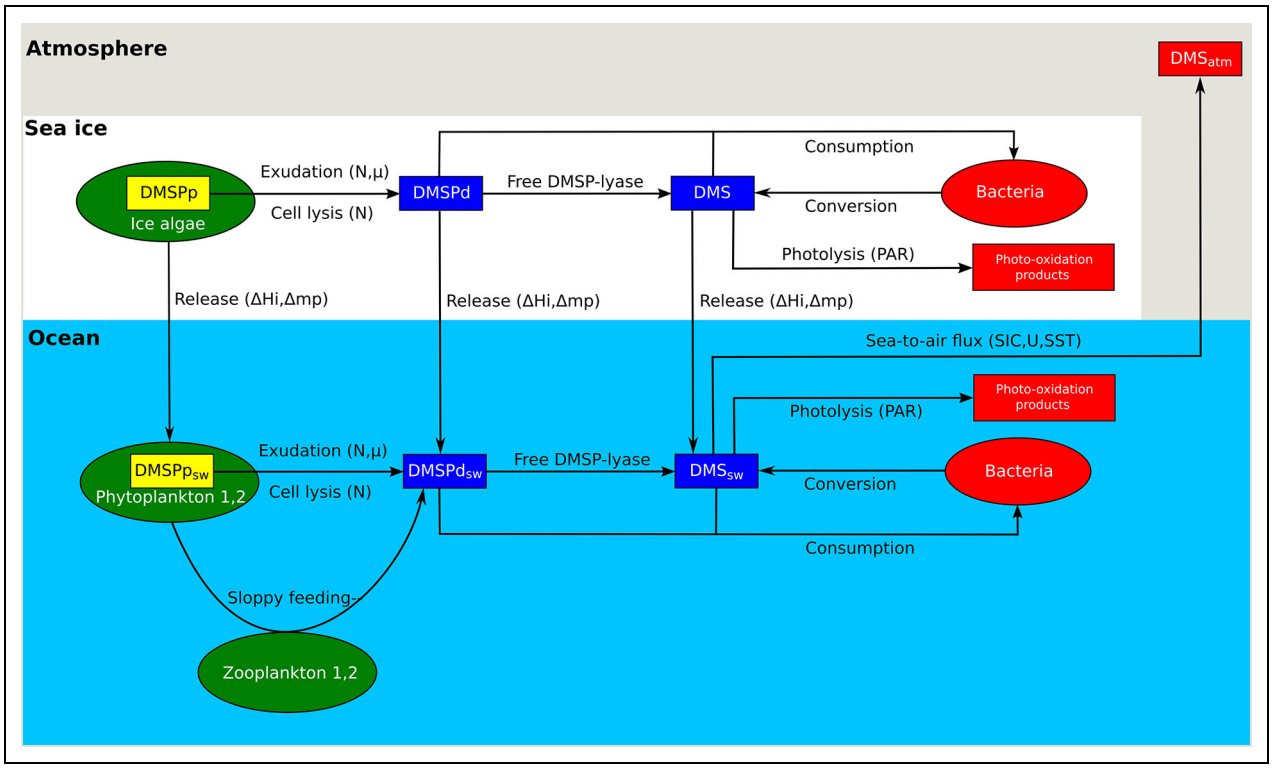

Figure 2. Schematic of the sea-ice and oceanic components of the sulfur biogeochemistry model. Variables in blue are prognostic, variables in yellow are diagnostic and variables in red are not simulated but the relevant processes are parameterized. Variables in green are prognostic components of the ecosystem model. Arrows represent the physical and biogeochemical fluxes parameterized in the model with, in parentheses, the controlling factors of each process, where N denotes nutrients (NO_3, NH_4), μ the ice algal growth rate, ΔHi the change in sea ice thickness, Δmp the change in melt pond area, SIC the sea ice concentration, U the near-surface wind speed, and SST the sea surface temperature.

either consumed by bacteria, degraded by photolysis or vented to the atmosphere from the uppermost layer of the ocean. Details of the model equations and parameters can be found in Hayashida et al. (2020).

2.1.2. Daily DMS emissions

Using daily data of DMS emissions for our analysis is especially relevant considering the fast timescales of atmospheric sulfur chemistry, as DMS can be oxidized rapidly and has residence times of only a few days (Sellegri et al., 2024). However, with the length of the simulation analyzed here, storing model output at a daily frequency for all variables was not practical in the simulation we considered. The DMS sea-to-air flux was only saved with monthly means, but daily means were available for ocean surface DMS concentrations (DMS_{os}), sea surface temperature (SST), sea ice concentration (SIC), and near-surface wind speeds (U_{10}). We therefore re-computed daily DMS emissions F_{DMS} from these variables for the periods of analysis, using the same parametrization as the model simulation:

$$F_{DMS} = DMS_{os}(1 - SIC)^{0.4}\, k_{N00}(U_{10}) Sc(SST) \qquad (1)$$

Here Sc is the SST-dependent Schmidt number from Saltzman et al. (1993). The term $(1 - SIC)^{0.4}$ is used to account for the non-linear relation between sea ice concentration and sea-to-air flux. This dependence on SIC represents the increase in gas transfer velocity that occurs at high sea ice concentrations due to enhanced convection below leads, as identified by Loose et al. (2009). This parametrization of the DMS sea-to-air flux is based on the gas transfer velocity from Nightingale et al. (2000), which considers a quadratic wind speed dependence: $k_{N00}(U_{10}) = 0.333U_{10} + 0.222U_{10}^2$.

To estimate the errors introduced by recomputing DMS emissions, we compared the monthly means saved directly during the simulation and monthly means calculated from the recomputed daily DMS emissions. We found relative root-mean-square differences of less than 17% and a systematic bias with recomputed values consistently overestimating monthly means directly saved by the model (Figures S1 and S2). These differences can be attributed to the non-linear dependence of DMS emissions on wind speed and sea ice concentration. Although these errors are not negligible, they can be deemed acceptable for the study of mechanisms controlling DMS emissions. However, when considering future projections and comparing our simulation with CMIP6 models or observation-based data products, we used the monthly means directly saved by the model.

Other gas transfer parametrizations have been proposed, and Zavarsky et al. (2018) found that a linear wind speed dependence best fit the observational data they collected, similarly to Marandino et al. (2007): $k_{Z18}(U_{10}) = 2.0U_{10} + 0.94$. We also re-computed daily DMS emissions with the parametrization from Zavarsky et al. (2018) to assess the sensitivity of DMS emissions to the choice of parametrization. Because the simulation we used was originally run using k_{N00} and re-computing DMS emissions with k_{Z18} can lead to inconsistencies, these data were used only as a first assessment of sensitivity.

2.1.3. Simulations

We focused our analysis on a simulation from 2016 to 2085 under a scenario of strong warming, representative concentration pathway (RCP) RCP8.5 (van Vuuren et al., 2011). We also considered a simulation forced with RCP4.5, a scenario with reduced emissions compared to RCP8.5, to investigate scenario uncertainty. These runs were initialized from the historical run previously analyzed in Hayashida et al. (2020). For the simulations studied here, the atmospheric forcing used was derived from the Canadian Regional Climate Model (CanRCM4) and the Canadian Earth System Model version 2 (CanESM2; Arora et al., 2011). Lateral boundary conditions are from CanESM2 (Arora et al., 2011) or are fixed to the same constant values used for the historical run (Hayashida et al., 2020). Further details regarding the simulation setup can be found in Haddon et al. (2024), where the RCP8.5 simulation has been analyzed focusing on the future of sea ice algae.

Surface and lateral forcings from CanRCM4 or CanESM2 were adjusted to account for model biases. Corrections were made by adding the anomaly between modeled and observed climatologies to the future forcing daily time series, as described in Haddon et al. (2024). Note, however, that these corrections were not carried out for the near-surface wind forcing, as the method used was found to result in unrealistic wind directions. Thus, there is a discontinuous transition in the wind forcing between the historical and future simulations, as well as a step change in DMS emissions between these two simulations as a result of the strong dependence of the DMS sea-to-air flux on wind speed. For these reasons, we analyzed the future run independently of the historical simulation, as changes in DMS emissions would be strongly affected by the change in wind forcing.

Changes were analyzed between the present, defined as the period 2016–2035, and the late 21st century, defined as the period 2066–2085. When presenting time series, we also plotted 20-year rolling means computed with 20 years of data centered around the year of interest, with shorter averaging periods using the available data at the start and end of the simulation.

3. Results

3.1. DMS emissions

We begin the presentation of these results with an analysis of DMS emissions, focusing on spatial and temporal variability. To assess when and where the simulated DMS emissions have a potential impact on climate, we considered the benchmark identified by Pandis et al. (1994). Using a simple steady state model of atmospheric sulfur (S) chemistry, they found that for DMS sea-to-air fluxes greater than 2.5 μmol S m^{-2} d^{-1}, there is a linear relationship between the cloud condensation nuclei (CCN) number concentration and the DMS flux. This relationship suggests that above this benchmark, DMS emitted from the ocean has an impact on cloud formation, and

therefore this reference value can be used as a benchmark in assessing DMS emissions. Note that the model used by Pandis et al. (1994) did not account for other sources of CCN and therefore this benchmark is only meaningful for remote regions where the atmosphere is not influenced by other aerosols, such as land emissions or sea spray. Furthermore, although evidence suggests that DMS is the main secondary source of aerosols in remote regions of the Arctic, there are other sources of aerosols that can impact the sensitivity of CCN formation to DMS emissions (Willis et al., 2018; Abbatt et al., 2019).

Throughout the Arctic, the model simulates an overall increase of the climatological mean May–August DMS emissions from present 2016–2035 to late 21st century 2066–2085 (**Figure 3a**–**c**). Time series of regional averages (**Figure 3g**) confirm that this increase is robust to the choice of climatological period. This increase is primarily the result of a northerly progression of areas with May–August mean DMS sea-to-air fluxes greater than 2.5 μmol S m^{-2} d^{-1}. Indeed, in the present, large mean DMS emissions occur mainly at lower latitudes and are found in the high Arctic only in a few small areas. However, by late century, DMS emissions in high latitudes regions, from the Chukchi to the Kara seas, increase substantially and become comparable to those of the Greenland, Iceland, Norway (GIN) and Barents seas.

The Arctic can be split into three groups of regions in terms of simulated DMS emissions (**Figure 1**). The first group is the Atlantic Arctic, composed of the GIN and Barents seas, where the regional average DMS sea-to-air fluxes are high in the present and increase only moderately by late century. In these regions, there is substantial spatial variability in the changes of DMS emissions, with strong increases at high latitudes compensating decreases in coastal areas at lower latitudes.

The second group, the Eastern Arctic, spans the large continental shelves of the Chukchi, East Siberian, Laptev, and Kara seas. Here, the moderate DMS emissions of the present increase substantially and by late 21st century, the highest DMS sea-to-air fluxes of the Arctic are simulated in these regions, notably in the Chukchi Sea.

Third is the Central and Western Arctic, comprising the deep basins of the Central Arctic and the Beaufort Sea as well as the narrow passages of the CAA and Baffin Bay. In these regions, mean DMS emissions are low in the present and remain low throughout the 21st century (**Figure 3**).

3.1.1. Temporal variability of DMS emissions

Substantial interannual variability is simulated, as shown in the interdecile range of May–August mean DMS emissions (**Figure 3d**–**f**). For both present and future periods, the highest inter-annual variability is simulated in areas of strong mean DMS emissions. A noteworthy exception is the coast of the East Siberian Sea during the present period, where despite low mean DMS sea-to-air fluxes, a large interdecile range reveals the existence of years of high DMS emissions. In the Chukchi Sea, the substantial increase in DMS sea-to-air fluxes from present to late century coincides with a strong increase of interannual variability. This result indicates that by late century, this region could have years with extremely high DMS emissions, as seen in the regional time series (**Figure 3g**).

Histograms of regional and daily mean DMS emissions for May and August (**Figure 4**) reveal that there is also strong temporal variability at subseasonal time scales. These distributions cover a wide range of values, even in regions with low mean DMS emissions, which shows that extreme events corresponding to bursts of DMS emissions are simulated. In the most productive areas, such as in the Atlantic Arctic during May, daily DMS sea-to-air fluxes can reach up to 10 times the benchmark of 2.5 μmol S m^{-2} d^{-1}. In the Central Arctic, DMS emissions greater than the benchmark of 2.5 μmol S m^{-2} d^{-1} are simulated, albeit with low probability, illustrating rare occasions of potential impact on CCN formation even where mean DMS emissions are low. The occurrence of these high-flux events also increases by late 21st century, particularly in both May and August for the Eastern Arctic and in May for the Atlantic Arctic. As discussed above, the benchmark DMS flux of 2.5 μmol S m^{-2} d^{-1} is not equally relevant at all locations. From **Figure 4**, in all regions in May and in all but a few in August (Baffin Bay, Kara Sea, GIN Seas), the frequency of daily DMS emissions exceeding any threshold greater than the benchmark value increases by late century. In this way, the increased frequency of DMS emissions bursts in the Arctic is robust.

To understand the drivers of the temporal variability of DMS emissions, we computed the power spectra of the regional and daily mean DMS emissions, ocean surface DMS concentrations and surface wind speed. Spectra were computed for each year and then averaged over 20 years for both periods (**Figure 5**). For DMS emissions, the spectrum displays power at both high and low frequencies, in all three groups of regions. High frequencies, with periods less than 7 days, correspond to short bursts of emissions, whereas low frequencies represent seasonal variations. The surface wind speed spectra are dominated by high frequency variability, concentrated around periods of a few days, corresponding to synoptic scale weather. Ocean surface DMS concentrations vary on longer time scales and are dominated by a seasonal cycle, resulting in a spectrum with most of the power in the low frequencies. Similarly, the sea ice annual cycle results in a spectrum concentrated in low frequencies (not shown). This spectral analysis indicates that the high frequency events of DMS emissions, such as bursts of emissions, are primarily controlled by wind variability. In contrast, the annual cycle of DMS emissions is the result mainly of the seasonal variations in ocean surface DMS concentration and sea ice cover.

3.1.2. Annual cycle of DMS emissions

We next analyze the annual cycle of DMS emissions (**Figure 6**), and how it changes in relation to changes in the physical drivers, sea ice cover and wind speed (**Figures 7**–**9**), and in ocean surface DMS concentration (**Figure 10**). DMS concentrations will be analyzed in Section 3.2.2.

In the Atlantic Arctic, the annual cycle of DMS emissions is dominated by a spring peak that increases in magnitude only moderately from present to late

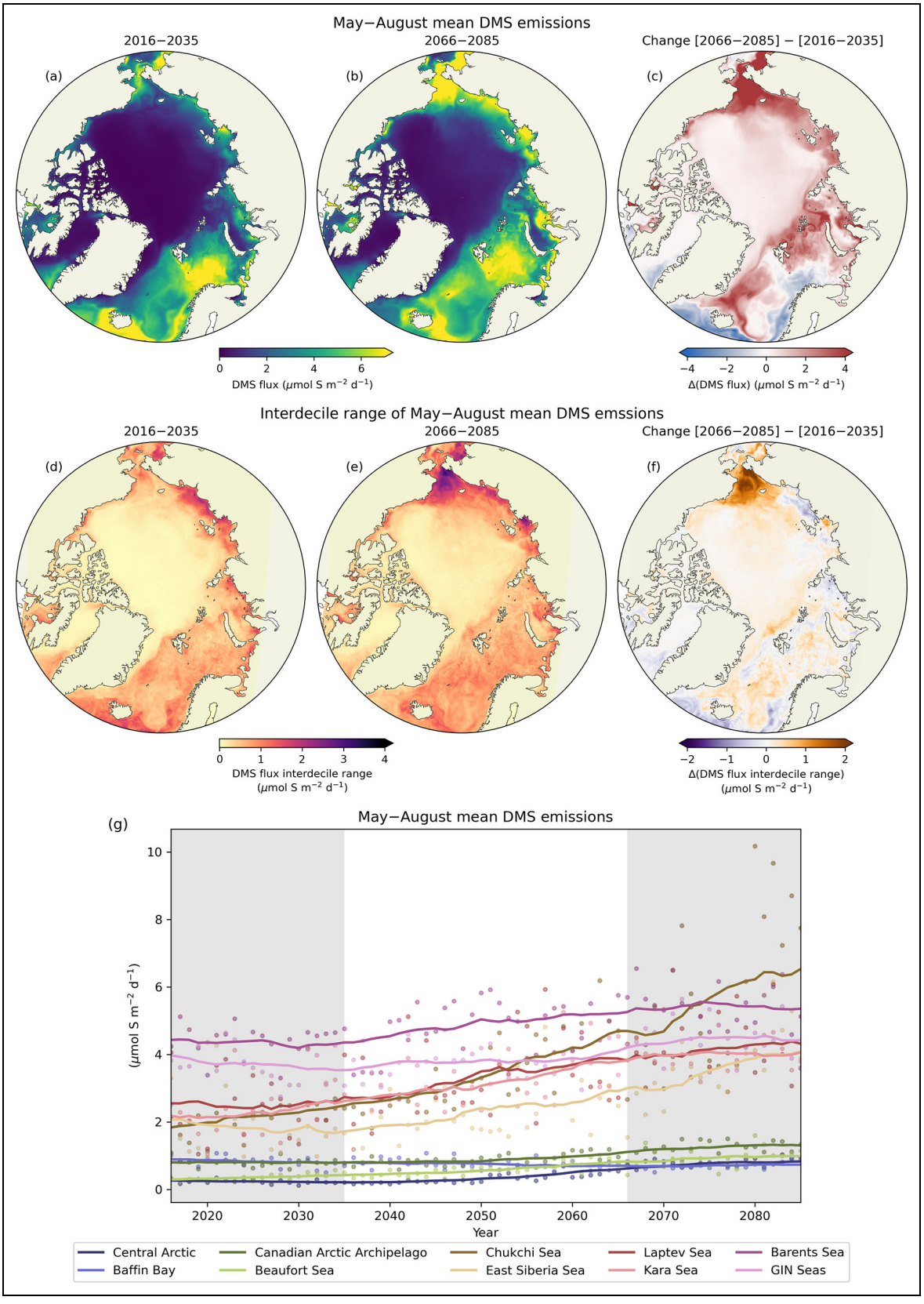

Figure 3. May–August DMS emissions. (a, b) Climatological May–August mean DMS emissions from present 2016–2035 and late 21st century 2066–2085 and (c) associated change. (d, e) Interdecile range of May–August mean DMS emissions and (f) associated change. (g) Time series from 2016 to 2085 of regional averages of May–August mean DMS emissions (dots) and 20-year rolling mean (lines).

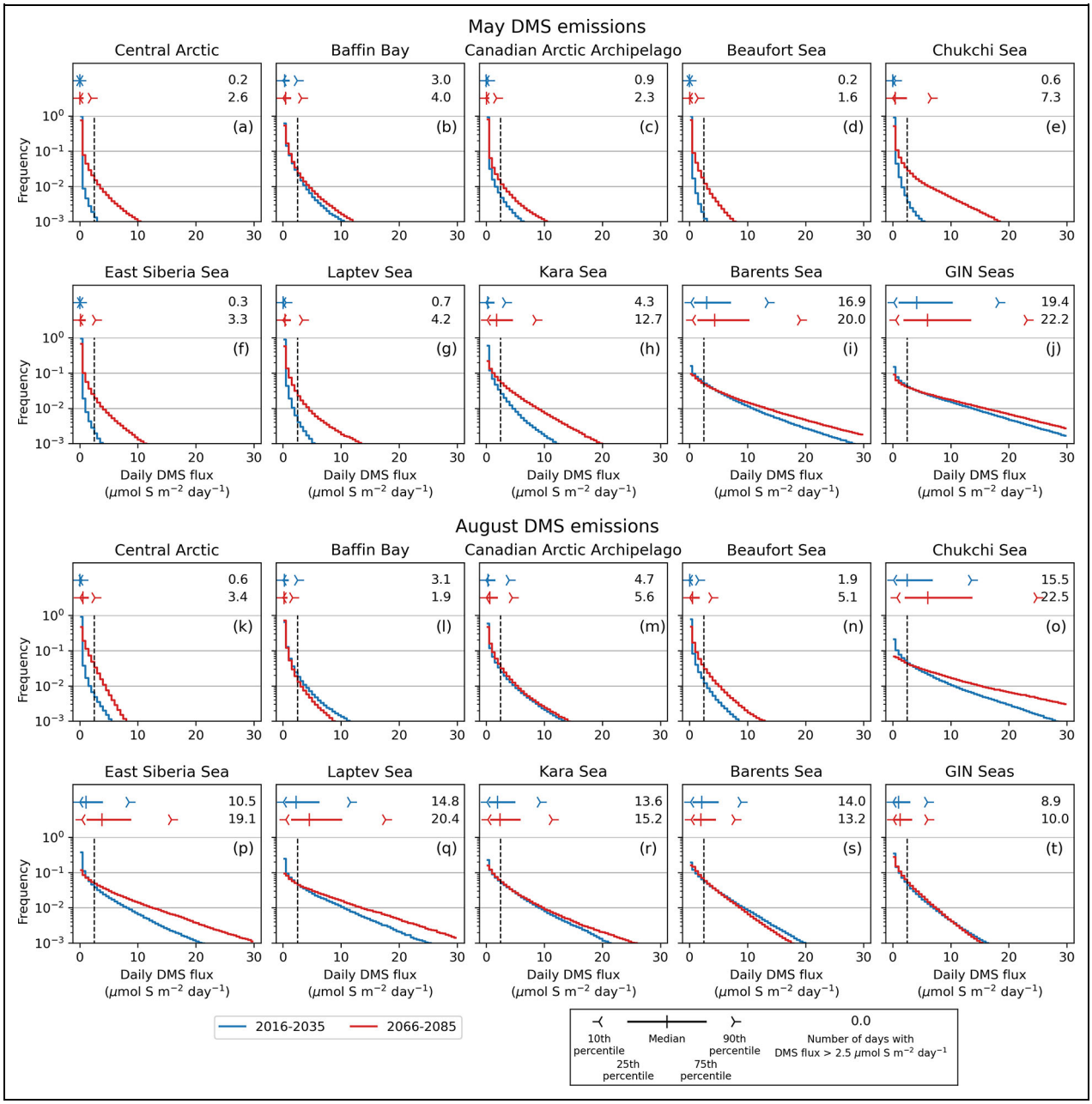

Figure 4. Temporal distribution of DMS emissions by region. Regional histograms and quantiles for May (a–j) and August (k–t) of DMS emissions, computed from 20 years of daily regional means, for the present 2016–2035 and late 21st century 2066–2085. At the top of each plot, the median, the 10th, 25th, 75th, and 90th percentile of the daily mean DMS emissions are displayed for both periods. Also shown is the average number of days when DMS emissions are greater than the benchmark of 2.5 μmol S m^{-2} d^{-1}, with the dashed vertical line corresponding to this benchmark.

21st century. The model simulates almost ice-free conditions in May already in the present (**Figure 8**), and thus DMS sea-to-air fluxes are not limited by the presence of sea ice. DMS emissions are therefore controlled by ocean surface DMS concentrations, and little change to the timing of DMS emissions is projected by the model as the onset of DMS production is already limited by the seasonal cycle of surface irradiance in the present. Although changes in the physical drivers result in increased gas transfer velocities throughout these regions, they do not lead to higher DMS fluxes everywhere. Notably, in the eastern Barents Sea, despite increases in the mean May wind speed (**Figure 8**), the DMS emissions decrease by late 21st century because of low ocean surface DMS concentrations (**Figure 10d–f**). In both periods, summer DMS emissions are lower than during spring, as a result of reduced ocean surface DMS concentrations. A minor fall DMS emissions peak occurs in September when wind speeds start to increase.

In the Eastern Arctic, spring DMS emissions are strongly limited in both periods by a substantial sea ice cover. As May sea ice concentrations are high, even in the

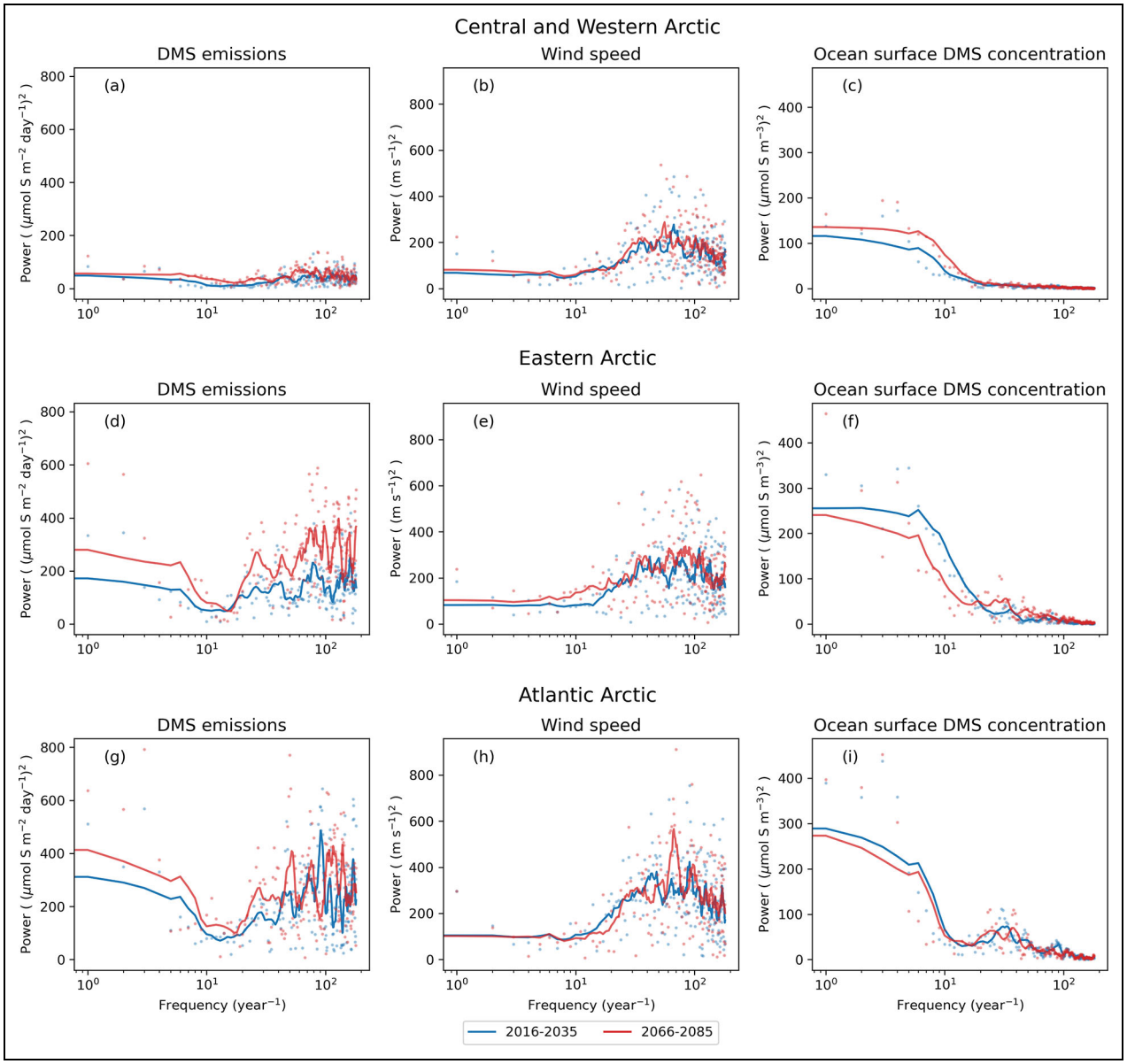

Figure 5. Power spectral density of daily DMS emissions, wind speed and ocean surface DMS. Power spectra of DMS emissions (a, d, g), 10 m wind speed (b, e, h) and ocean surface DMS concentration (c, f, i), for the Central and Western Arctic (a–c), Eastern Arctic (d–f) and Atlantic Arctic (g–i). The spectra $S(f)$ are computed using the fast Fourier transform (FFT) from daily time series of regional means for each year, for frequencies f up to 180 y^{-1}. We plot here the product $fS(f)$ averaged over 20-year periods (dots) and the rolling mean over 10 frequencies (lines), for the present 2016–2035 and late 21st century 2066–2085.

late 21st century (**Figure 8e**), the substantial spring DMS production from ice algae and under-ice blooms is trapped below the ice (**Figure 10**). Future DMS emissions start earlier in the year but remain largely below the benchmark of 2.5 μmol S m^{-2} d^{-1} during spring. Once sea ice begins to retreat, DMS emissions become substantial, with high emissions simulated until September. Summer DMS emissions and ocean surface concentrations increase strongly from present to late 21st century and are associated with a total loss of sea ice cover in August. Peak DMS emissions occur earlier in the future, and these changes in timing are linked not only to earlier sea ice break-up but also to earlier DMS production. Summer surface wind speeds increase from present to late 21st century, and in particular the monthly 90th percentile wind speed shifts higher (**Figure 7e–h**), resulting in a greater occurrence of strong bursts of DMS emissions (**Figure 4**).

In the Central and Western Arctic, DMS emissions are low throughout the year, with only a moderate increase in magnitude and a small change in timing from present to late 21st century. A spring peak in DMS concentrations is clearly noticeable, with ocean surface DMS reaching concentrations comparable to areas at lower latitudes with higher emissions, such as in the Eastern Arctic. However, spring DMS emissions are blocked by a substantial sea ice cover in both periods, as the model simulates little changes in the May sea ice concentration before 2085

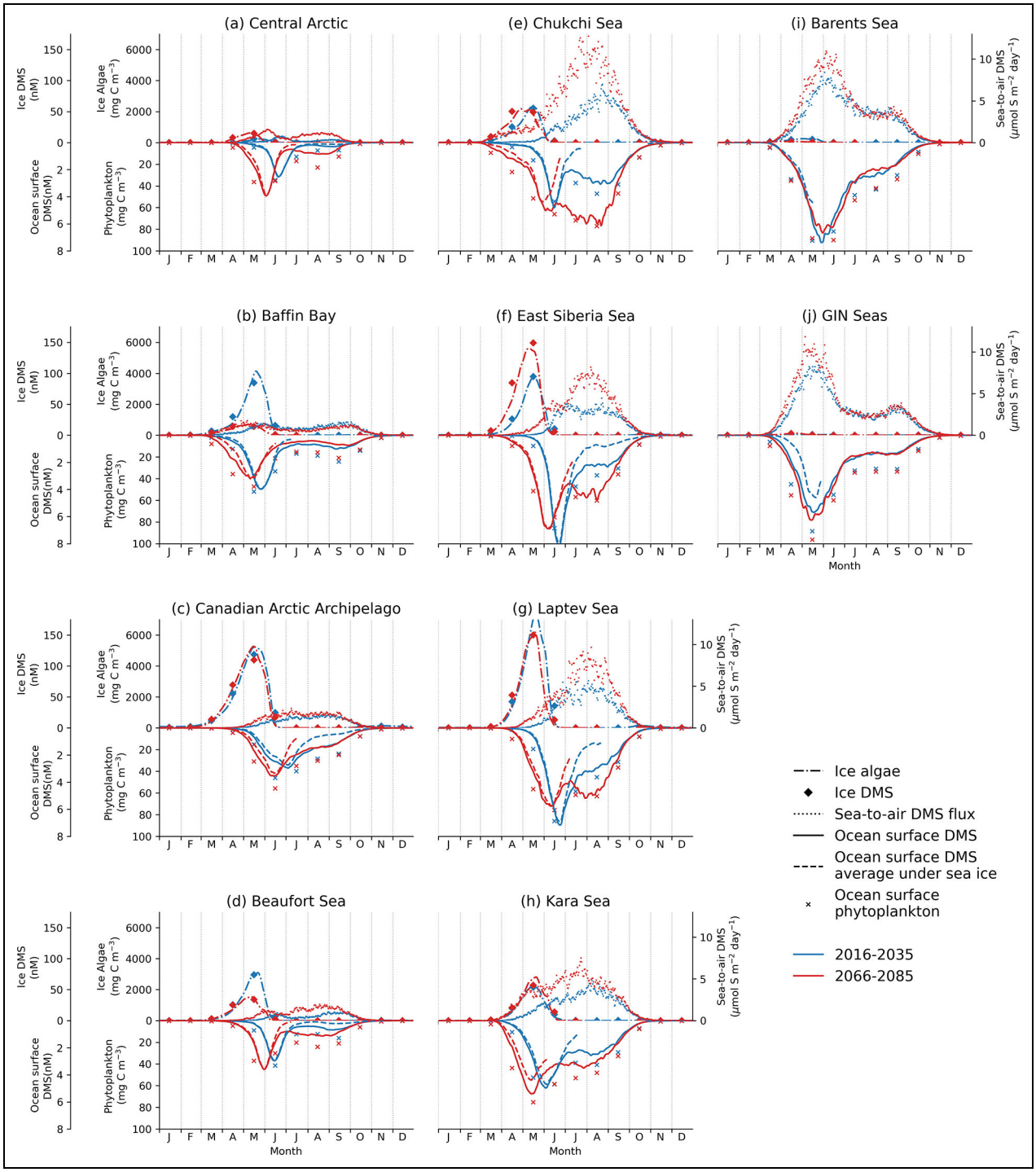

Figure 6. Ice and ocean surface DMS concentrations and emissions: 20-year mean annual cycles of regional averages. Annual cycle of daily DMS sea-to-air flux (dots), daily ice algal biomass (dashed-dottted lines), monthly sea ice DMS concentration (diamonds), daily ocean surface DMS concentration (full and dashed lines), and monthly ocean surface phytoplankton biomass concentration (crosses). For the ocean surface DMS concentration, both the regional average (full lines) and the under-ice regional average (dashed lines) are shown, where under-ice is the area with a sea ice concentration greater than 50%. Climatological averages computed over 20 years, for the present 2016–2035 and late 21st century 2066–2085. Left column (a–d) are regions of the Central and Western Arctic, center column (e–h) are regions of the Eastern Arctic, and right column (i, j) are regions of the Atlantic Arctic.

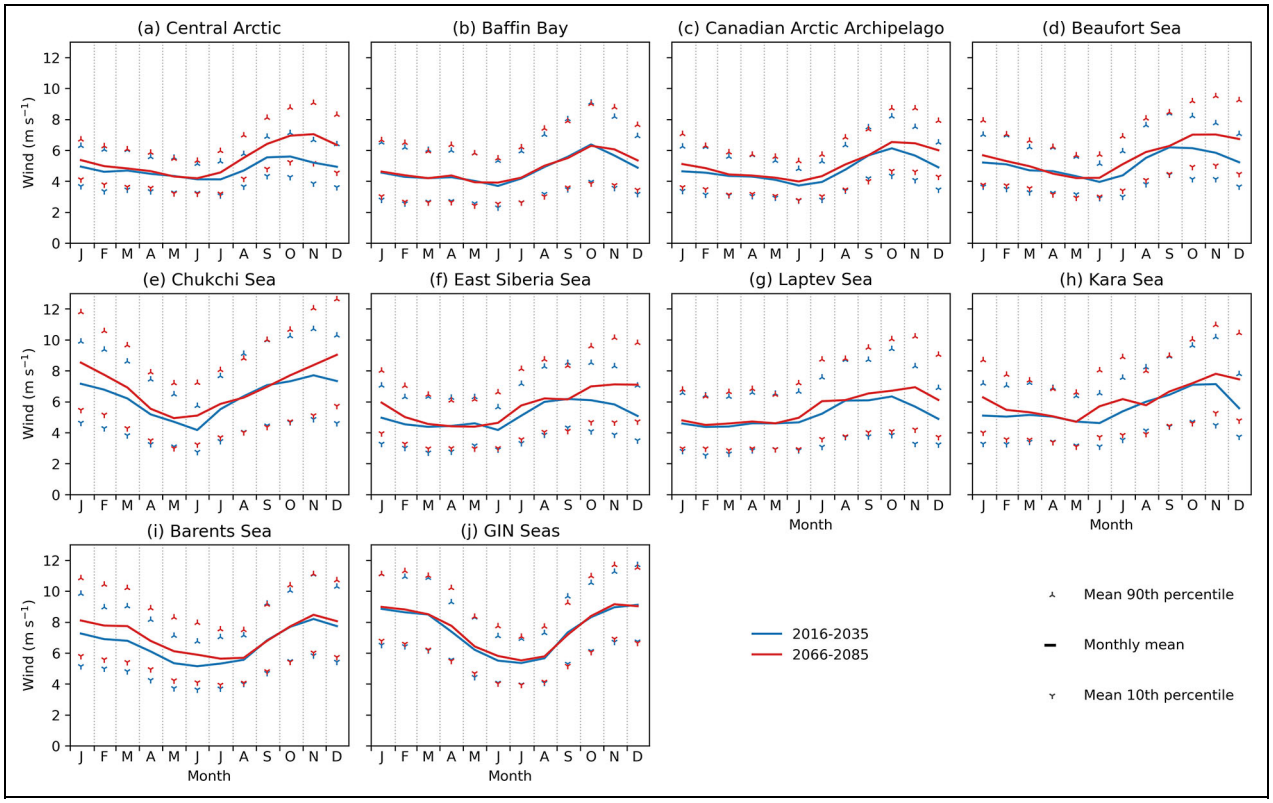

Figure 7. Surface wind speed: 20-year mean annual cycles of regional averages. Monthly mean and monthly 10th and 90th percentiles of the surface wind speeds, computed from daily regional means. Climatological averages computed over 20 years, for the present 2016–2035 and late 21st century 2066–2085.

(**Figure 8**). In contrast, late summer emissions are limited mainly by a lack of DMS production (**Figure 10**), in particular in the late 21st century, when the model simulates ice-free conditions in August and an associated increase in mean wind speed (**Figure 9**). Nonetheless, summer DMS emissions increase in the Central Arctic and the Beaufort Sea and in the future some areas show up to 10 days in August, with fluxes greater than the benchmark of 2.5 μmol S m^{-2} d^{-1}(**Figure 9b**). Moreover, in the CAA and along the Beaufort shelf, there are small areas of large summer DMS emissions, and by late 21st century DMS fluxes in these areas almost always exceed 2.5 μmol S m^{-2} d^{-1}.

Throughout the Arctic, there are only small changes to fall DMS emissions in September and October (**Figure 6**). This result can be linked to the absence of changes in the fall DMS ocean surface concentration. As a result, there is no extension of the period with substantial DMS emissions, despite freeze-up occurring later by late 21st century.

3.2. DMS concentrations

3.2.1. Biological control

To assess the relation between phytoplankton biomass and DMS concentrations, we carried out linear regressions of regional mean ocean surface DMS concentrations on ocean surface total phytoplankton biomass. Despite the detailed representation of a variety of sulfur cycle processes in the model, there is a strong correlation between DMS concentrations and phytoplankton biomass. The strength of this correlation is indicated by consistently high coefficients of determination r^2 values, greater than 0.8 during the productive period from March to October (Figure S3).

Figure 11 shows the monthly mean slopes obtained from the DMS-biomass linear regressions. These slopes have units of DMS concentration per unit of phytoplankton biomass and can be interpreted as the overall DMS production efficiency of the pelagic ecosystem. Although there is a strong correlation between DMS concentration and phytoplankton biomass, the slope of this relation changes substantially between regions and seasons. An annual cycle of the DMS concentration to phytoplankton biomass slopes is clearly visible, following the annual cycle of primary production, with DMS production efficiency increasing strongly from spring to summer and decreasing in the fall. From present to late 21st century, a general increase in the DMS concentrations per unit of phytoplankton biomass is simulated. This increase is particularly noticeable in the regions of the Eastern Arctic where ocean surface DMS concentrations increase substantially (**Figure 6**).

The correlation between ocean surface DMS concentration and phytoplankton biomass can also be seen in the climatological annual cycles of these two variables, which exhibit the same patterns. Similarly, ice algal biomass and sea ice DMS concentration share the same overall annual cycles, indicating that they are also strongly correlated (**Figure 6**).

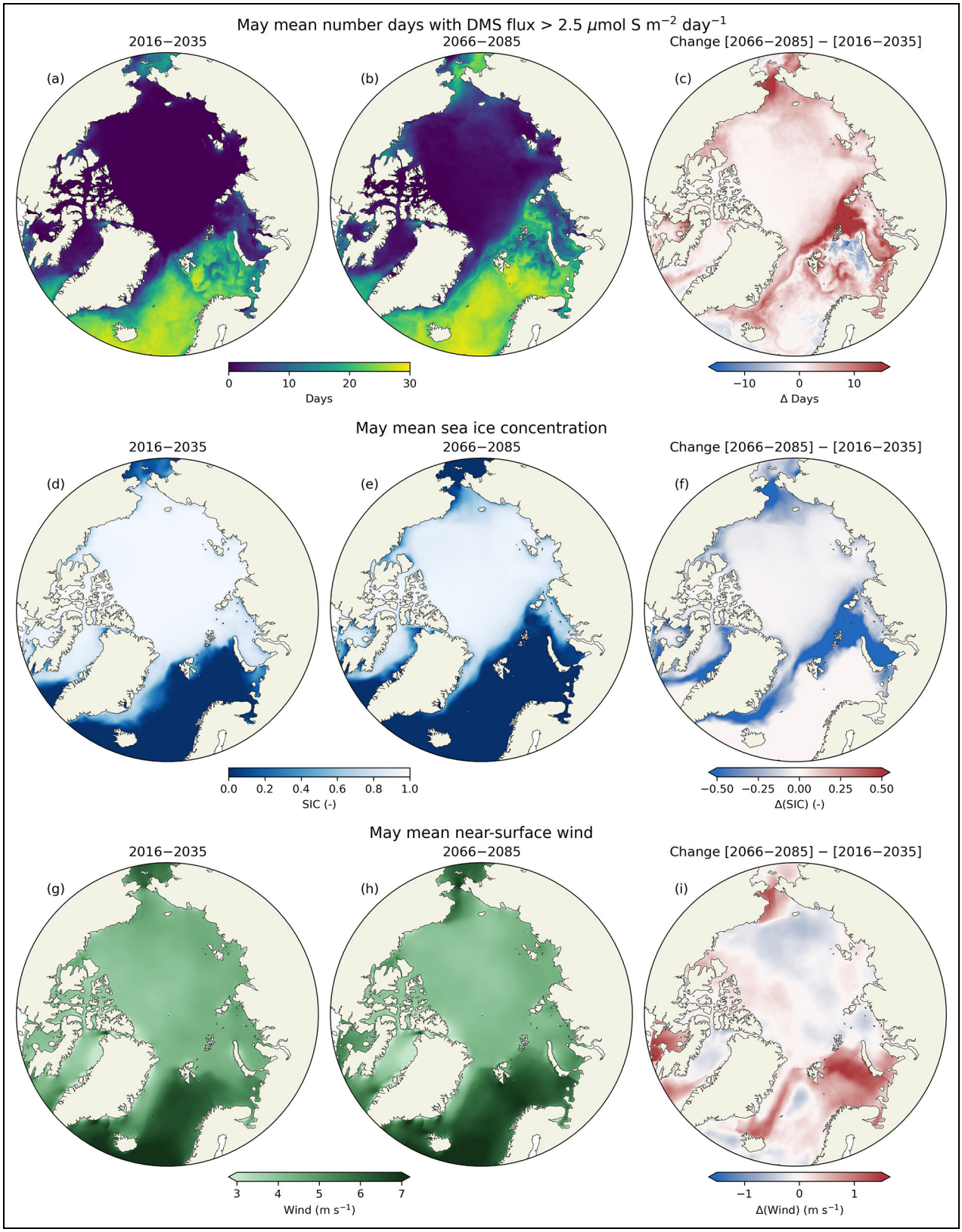

Figure 8. May DMS emissions and physical drivers. (a, b) Climatological mean number of days with DMS emissions greater than 2.5 μmol S m^{-2} d^{-1} in May and (c) associated change from present 2016–2035 to late 21st century 2066–2085. (d, e) Climatological mean May sea ice concentration and (f) associated change. (g, h) Climatological mean near-surface wind speed and (i) associated change.

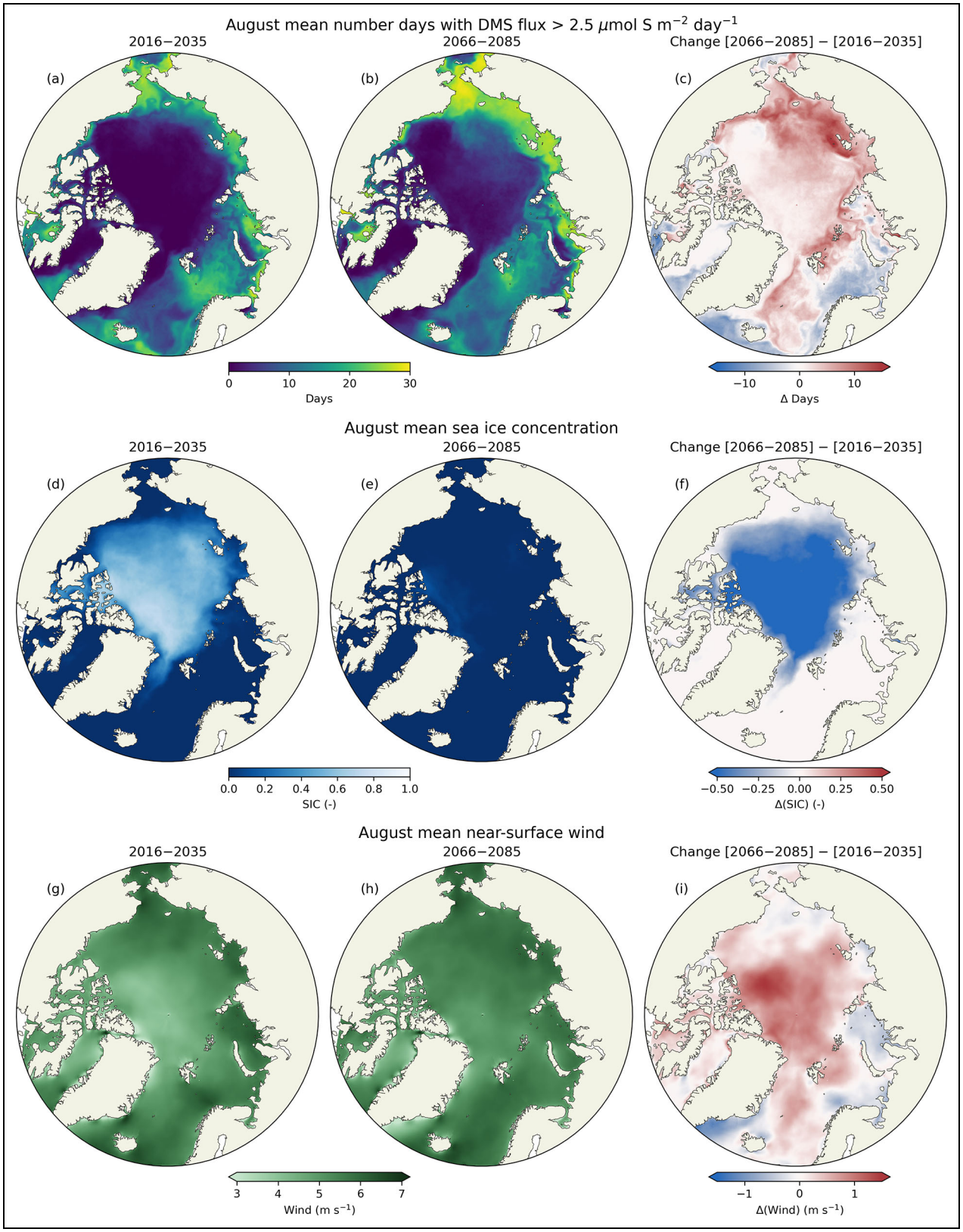

Figure 9. August DMS emissions and physical drivers. (a, b) Climatological mean number of days with DMS emissions greater than 2.5 μmol S m^{-2} d^{-1} in May and (c) associated change from present 2016–2035 to late 21st century 2066–2085. (e, f) Climatological mean May sea ice concentration and (g) associated change. (h, i) Climatological mean near-surface wind speed and (j) associated change.

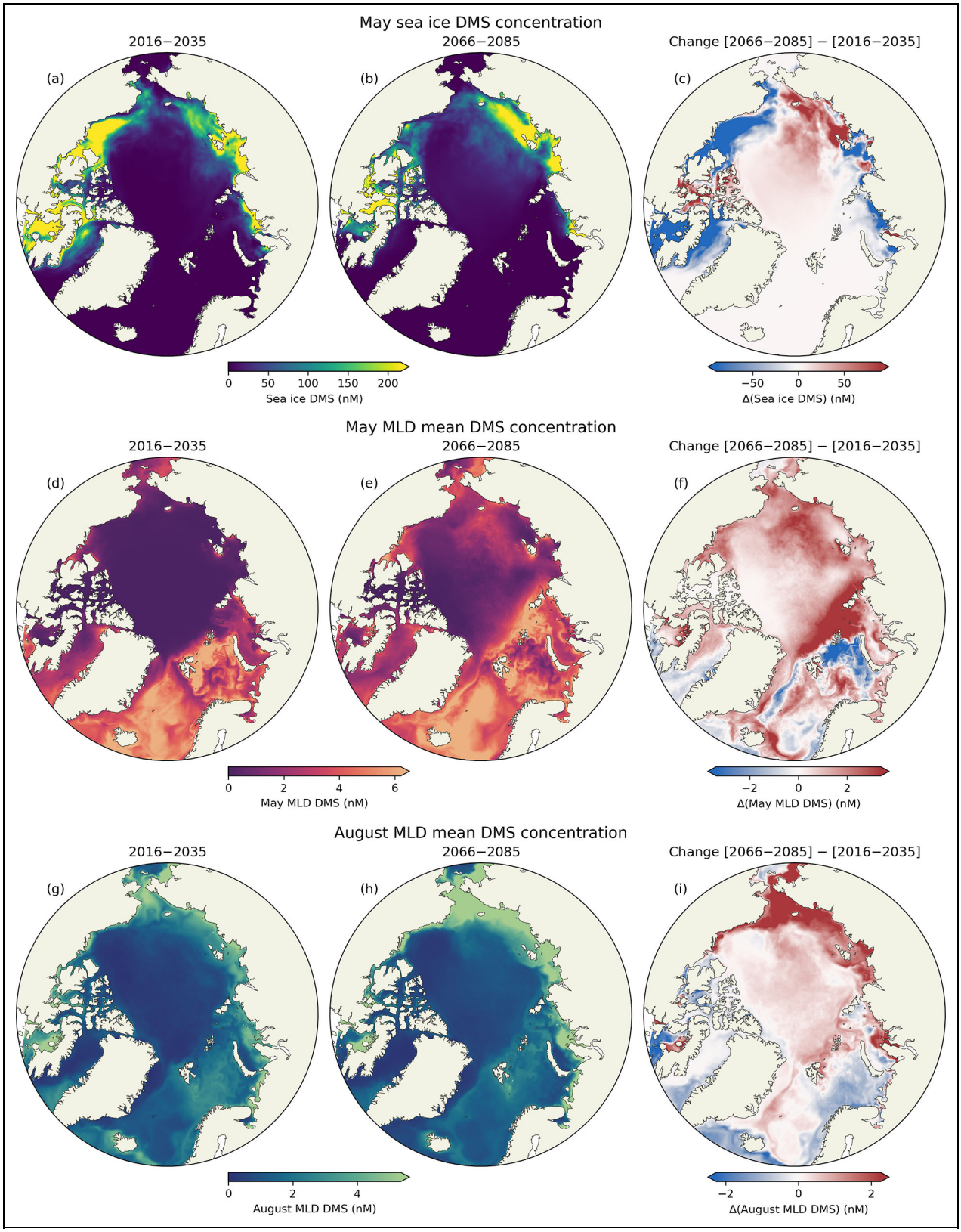

Figure 10. Ice and mixed layer mean DMS concentration. (a, b) Climatological mean sea ice DMS concentration in May and (c) associated change from present 2016–2035 to late 21st century 2066–2085. (d, e) Climatological mixed layer mean DMS concentration in May and (f) associated change. (g, h) Climatological mixed layer mean DMS concentration in August and (i) associated change.

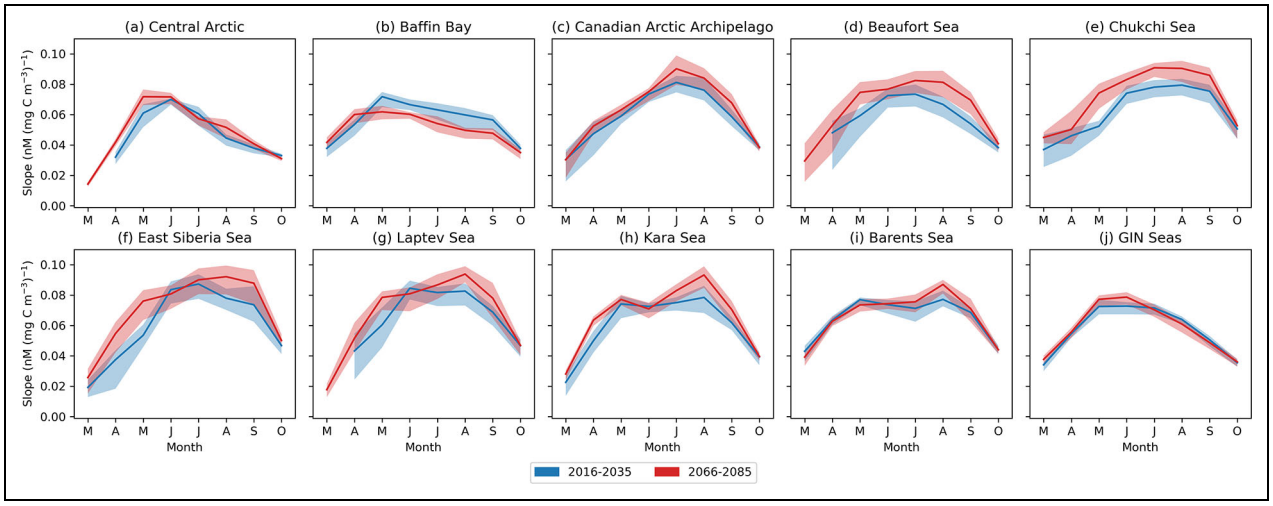

Figure 11. Slopes of ocean surface DMS versus phytoplankton relation. Slopes obtained from the linear regression of ocean surface DMS concentration as a function of ocean surface total phytoplankton biomass. Linear regressions were computed for each month of every year using model output from all grid cells of a given region. The 20-year monthly mean slopes are plotted, with shaded areas corresponding to the interdecile range over 20-year periods, for the present 2016–2035 and late 21st century 2066–2085. Values are plotted only when the mean r^2 of the linear regressions is greater than 0.8.

3.2.2. Annual cycle of DMS concentrations

During spring, DMS production at high latitudes begins in sea ice and closely follows primary production, with sea ice DMS concentrations reaching a maximum in May when ice algal biomass peaks. Both increases and decreases in May sea ice DMS concentrations are simulated from the present to the late 21st century (**Figure 10a–c**), with substantial reductions in the Beaufort Sea and Baffin Bay but a strong increase in the East Siberian Sea. In both periods, sea ice DMS concentrations reach high levels in productive regions and are up to one order of magnitude higher than ocean surface DMS concentrations. The accumulation of sea ice DMS in the late 21st century does not begin earlier in the year than in the present, except in the Chukchi and East Siberian seas where changes in the timing of sea ice DMS production are small compared to the large changes in sea ice (**Figure 6**). The absence of a major shift in the onset of sea ice DMS production is associated with only small changes in the timing of ice algal blooms. The low sensitivity of ice algal phenology has been attributed to a later sea ice freeze-up in the future, leading to a reduction of overwintering ice algae in model simulations (Haddon et al., 2024). The resulting lower initial biomass at the beginning of spring then causes a delay in the development of sympagic blooms, offsetting earlier light from thinner ice.

To analyze the annual cycle of DMS concentrations in the ocean, we plotted in **Figures 12**, S4, S5, and S6 the regional vertical profiles of DMS concentration along with the main controls of primary productivity, photosynthetic active radiation (PAR), and nitrogen. In contrast to what occurs in sea ice, the timing of DMS concentrations in the ocean responds to changes in sea ice thickness, with thinner sea ice in the future allowing for an increase in PAR earlier in the year and thus more favorable growing conditions during spring (**Figure 12**). As a result, under-ice DMS production begins earlier in the late 21st century in ice-covered regions, with more than a month change in the Chukchi Sea.

In addition to changes in timing, spring ocean DMS concentrations in sea ice-covered regions increase substantially from present to late 21st century (**Figure 10d–f**). **Figure 6** shows that the regional averages of ocean surface DMS concentration and averages restricted to under sea ice are very close until June in all regions of the Arctic, except for the Barents and GIN seas. This pattern indicates that in the high Arctic where sea ice cover remains extensive during spring even in the late 21st century, early DMS concentrations in the ocean are the result of under-ice blooms. Changes from present to late 21st century in May mixed layer DMS concentrations are therefore caused by earlier and more substantial under-ice blooms. This higher productivity can be linked to stronger winter mixing, leading to increases in ocean surface nitrogen concentrations at the onset of spring, notably in the Beaufort and Chukchi seas (**Figure 12**).

As the regions of the Atlantic Arctic are mostly ice-free already in the present, a strong pelagic bloom develops in the spring, and there is no change in the timing of the ocean surface DMS concentrations peak from present to late 21st century (**Figures 6** and **12**). In these regions, strong spatial variability is simulated with both areas of high and low May DMS concentrations in the late 21st century (**Figure 10d–f**). Mean surface wind speeds in May increase substantially over the 21st century (**Figure 8**), leading to a deep mixed layer throughout the Barents Sea (**Figure 13**). Strong spatial variability is also simulated in the May mixed layer depth (MLD), and although it is not apparent in the 20-year climatologies, it is clearly seen in individual years (not shown). Deep mixing dilutes the DMS produced in seawater over a greater depth, leading

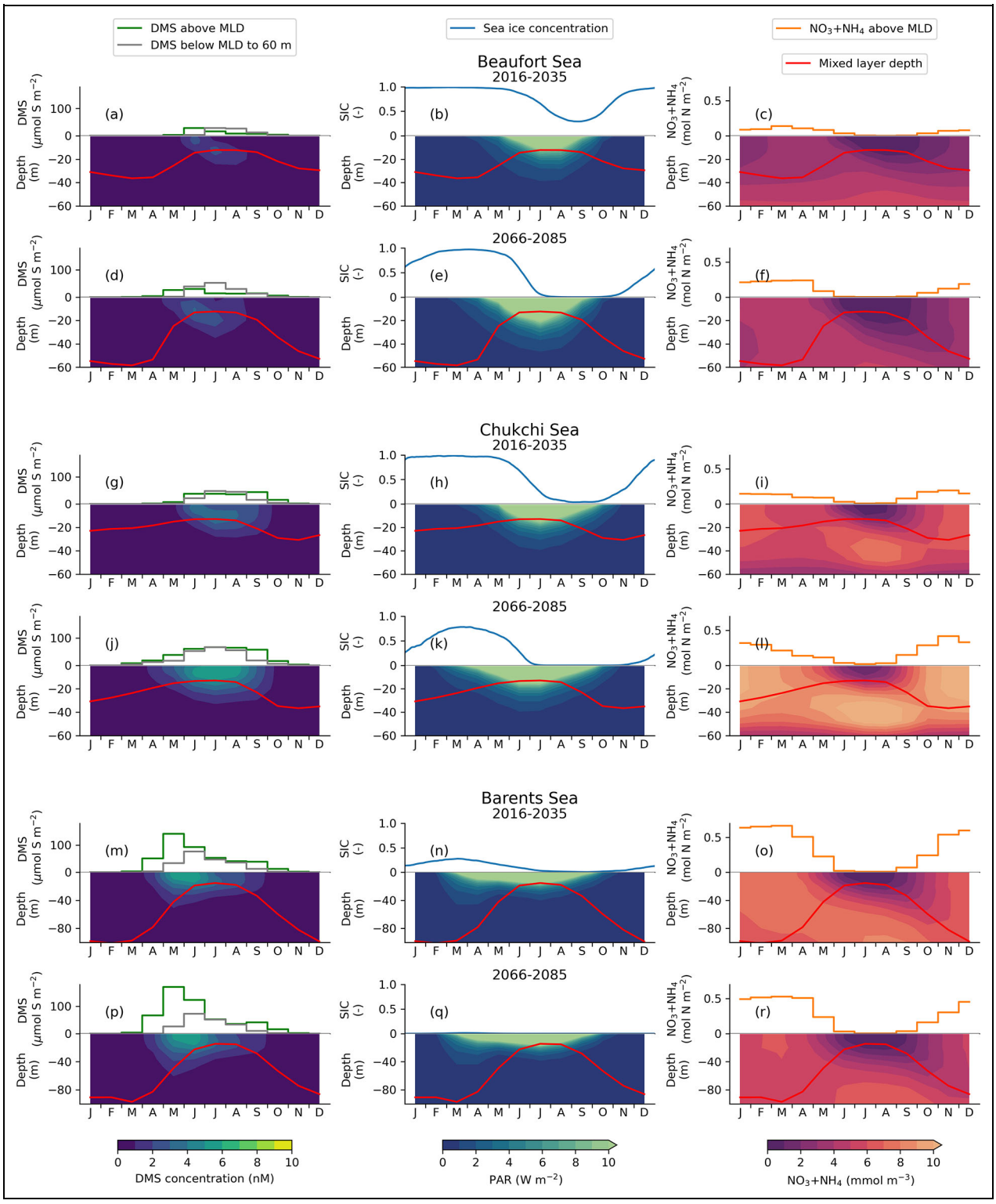

Figure 12. Annual cycles of vertical profiles. Annual cycles of regionally averaged vertical profiles of DMS concentration (left), photosynthetic active radiation (PAR, center) and total nitrogen (right), for the Beaufort, Chukchi, and Barents seas. Also shown is the regional mean mixed layer depth (MLD, red line), the vertically integrated monthly mean total DMS above the MLD (green) and below the MLD to 60 m (gray line), daily sea ice concentration (blue line) and vertically integrated total nitrogen above the MLD (orange line). Climatological averages computed over 20 years, for the present 2016–2035 and late 21st century 2066–2085.

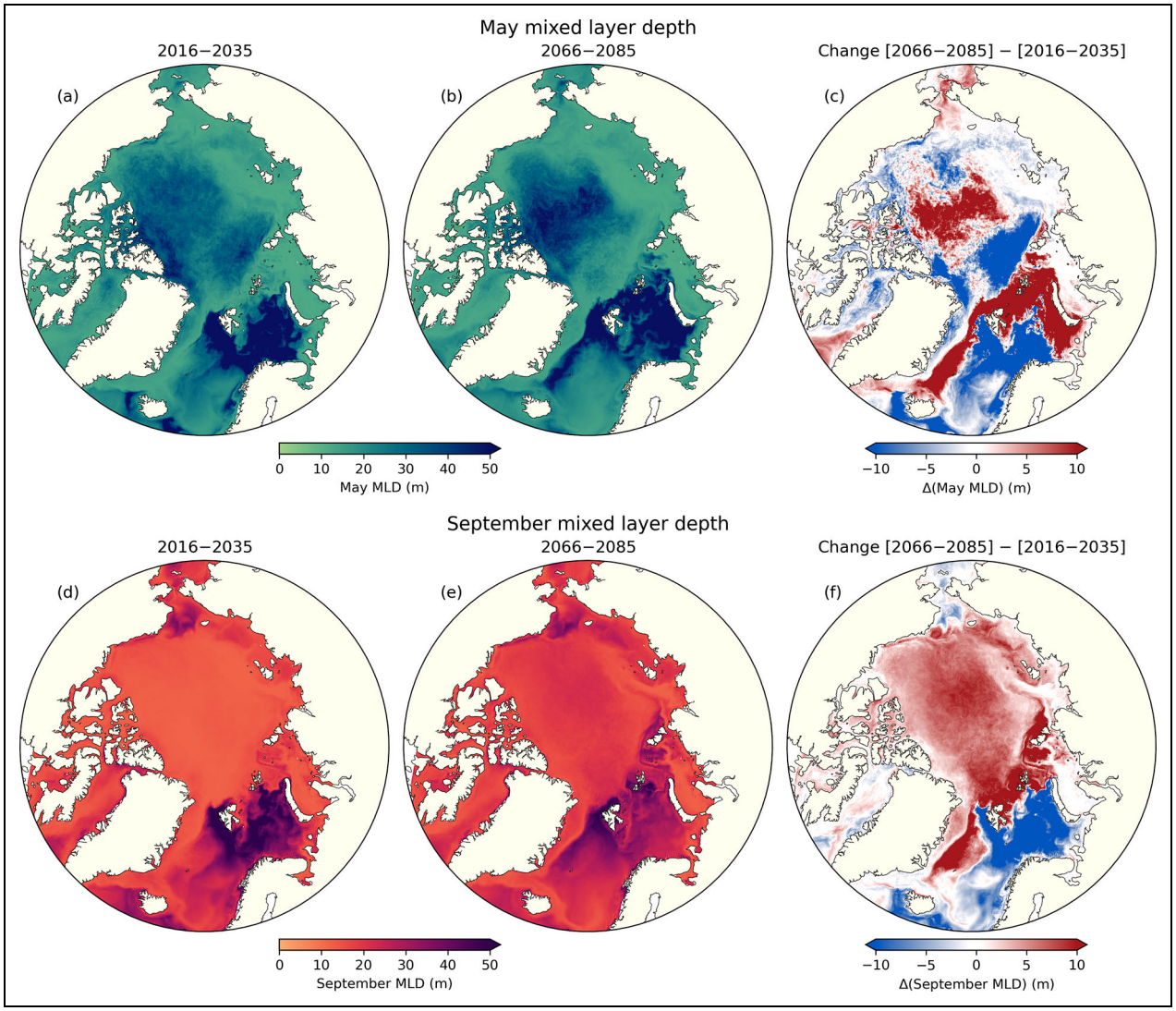

Figure 13. May and September mixed layer depth. Climatological mixed layer depth in May (a–c) and September (d–f). Climatological averages computed over 20 years, for the present 2016–2035 and late 21st century 2066–2085.

to a reduction of surface DMS concentrations. The role of dilution by vertical mixing is illustrated through consideration of total DMS integrated down to the MLD, which shows much less spatial variability and is high throughout the Barents Sea (Figure S7).

In the deep oceanic basins of the Beaufort Sea and of the Atlantic and Central Arctic, as well as in Baffin Bay, ocean surface DMS concentrations decrease strongly at the end of spring as surface nutrients become depleted (**Figures 12**, S4–S6). Primary production and DMS production can still occur at depth, where nutrients are available, and as a result deep chlorophyll and DMS maxima develop during summer. In ice-covered regions, this deepening of DMS production occurs earlier in the year by late 21st century, from earlier ocean surface blooms. As the mixed layer is particularly shallow in the Arctic during summer, substantial amounts of DMS are produced below the MLD. Comparing integrated DMS from the surface to the MLD and from the MLD down to 60 m (**Figure 12**) shows that the DMS stock below the MLD in these regions can be greater or equal than the DMS stock above the MLD. While this deep DMS stock represents a substantial source of DMS during summer, the DMS remains trapped at depth below the MLD instead of being ventilated to the atmosphere and thus does not lead to strong summer DMS emissions.

In the Eastern Arctic, such as the Chukchi Sea, in the present the ocean surface DMS concentration reaches a peak in June (**Figure 12**). However, on these shallow continental shelves, DMS production above the MLD continues during summer, as surface nutrient concentrations are depleted later in the year compared to other regions. Surface DMS concentrations are lower in August than in May due to higher sea-to-air fluxes from reduced sea ice concentrations. From present to the late 21st century a strong increase is simulated in the August MLD mean DMS concentrations (**Figure 10g–i**), and in the Chukchi Sea the annual peak in ocean DMS concentration shifts from June to August (**Figure 6**). This increase in summer DMS concentrations can be attributed to stronger winter mixing both locally and in upstream regions in the late 21st century, leading to higher surface nitrogen

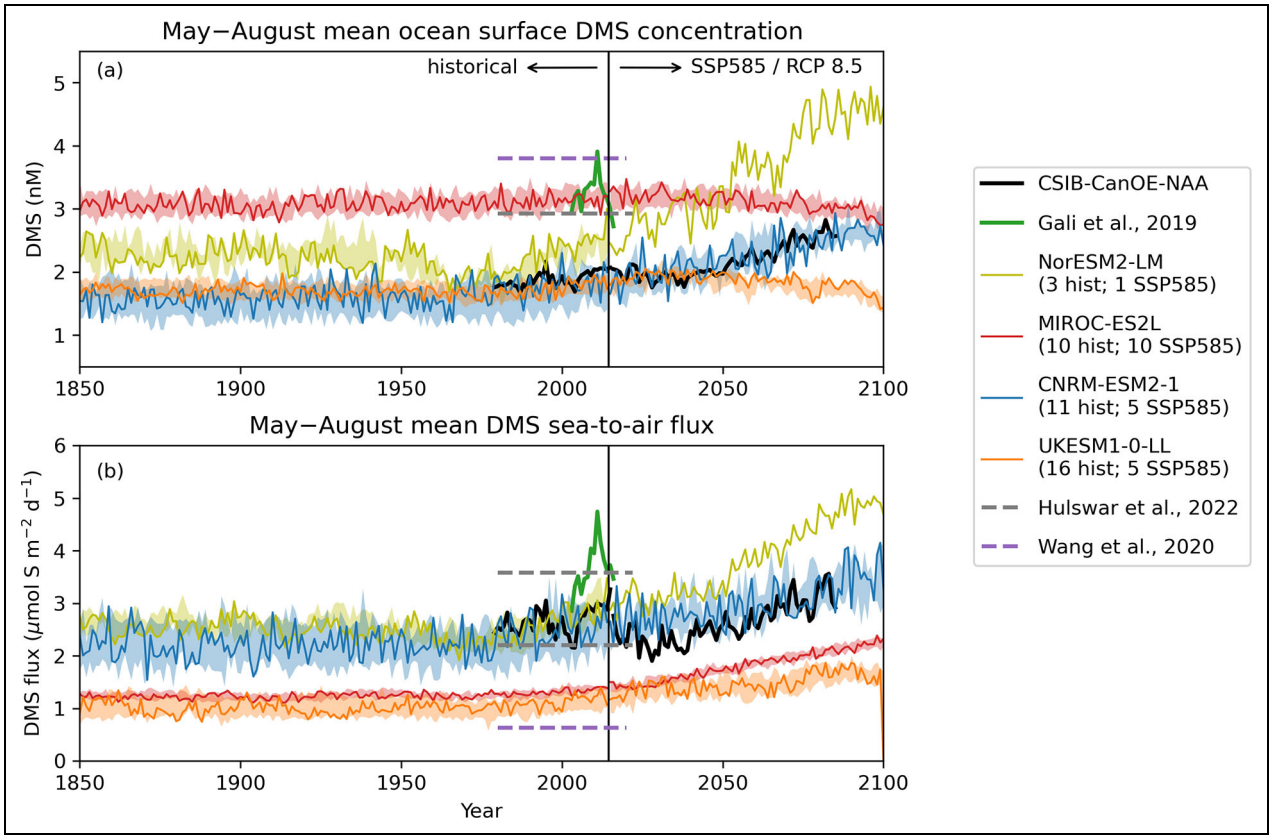

Figure 14. Comparison with other models and data products. May–August mean (a) ocean surface DMS concentration and (b) DMS sea-to-air flux, averaged over polar regions north of 70°N. This figure compares the model used in this study (CSIB-CanOE-NAA) with models participating in the Coupled Model Intercomparison Project (CMIP6) that computed ocean DMS (NorESM2-LM, MIROC-ES2L, CNRM-ESM2-1, UKESM1-0-LL) and observation-based data products (Galí et al., 2019; Wang et al., 2020; Hulswar et al., 2022). For CMIP6 models, lines correspond to a single simulation and shaded areas show the range of values across all ensemble members, with numbers in the legend indicating the size of the ensemble. The observation data products Wang et al. (2020) and Hulswar et al. (2022) are monthly climatologies, and the May–August means of these products are plotted as constant values over the time range of the observations used. For the DMS emissions from (Hulswar et al., 2022), we show both the climatological mean computed with and without a sea ice mask, the lower value corresponding to the mean with a sea ice mask.

concentrations (**Figure 12**). Nutrients above the MLD are therefore not completely depleted during summer in the future, and as a result sustained DMS production continues throughout summer. Moreover, substantial DMS production also occurs below the MLD in these regions in both periods, with similar integrated DMS quantities above and below the MLD in summer.

Throughout the Arctic, as the MLD deepens in the fall, surface nutrients are replenished and are no longer at growth-limiting concentrations. This transition occurs earlier in the year in the late 21st century, as indicated by a deepening of the September MLD in the future for most the Arctic (**Figure 13**). However, there is little impact on DMS concentrations which remain low in September in both the present and late 21st century. Instead, at high latitudes, the surface irradiance is the limiting factor, with light limitation beginning when PAR is below 4 W m^{-2} in the model, and thus the onset of light limitation of primary production occurs in late September (**Figure 12**). Furthermore, the deepening of the MLD in the fall exacerbates light limitation by reducing the mixed layer mean PAR.

4. Discussion

4.1. Future DMS emissions and concentrations

This study presents results from a single model driven by a single realization of atmospheric variability. As such it cannot directly quantify uncertainty associated with internal variability or choice of driving model. To put our analysis into perspective, we compared the model used here (CSIB-CanOE-NAA) with the four CMIP6 models incorporating oceanic DMS (NorESM2-LM, MIROC-ES2L, CNRM-ESM2-1, UKESM1-0-LL), and three observation-based data products (Galí et al., 2019; Wang et al., 2020; Hulswar et al., 2022). **Figure 14** presents pan-Arctic May–August means of DMS ocean surface concentration and DMS emissions. These various estimates of Arctic DMS concentrations and emissions show large differences, and observation-based data products also differ substantially. The spread in the estimate of mean DMS emissions from

observation-based data products is greater than from models for the same period, which can be attributed mainly to large differences in the sea ice masks used by the observation-based data products. For both DMS concentrations and emissions, models differ substantially in the characteristics of variability, with strong differences in interannual and decadal variability, as well as in the spread across ensemble members.

Despite the differences in historical DMS emissions, this comparison with CMIP6 models confirms the robustness of the increasing trend for pan-Arctic DMS emissions seen in the model analyzed here. Indeed, all CMIP6 models project an increase in DMS emissions, even for models which simulate a decrease in the mean ocean surface DMS concentration. Bock et al. (2021) showed that this trend is controlled primarily by the strong sea ice decline, which results in more surface area for air-sea gas exchanges by the end of the 21st century. This correlation between DMS emissions and sea ice area is also reinforced by model parametrizations, as all CMIP6 models scale DMS emissions linearly with sea ice concentration. However, recent studies challenge this simple relationship. Firstly, a partial sea ice cover can have an effect on interfacial turbulence thereby impacting air-sea fluxes, as confirmed by field observations showing that gas transfer velocities scale non-linearly with sea ice concentration (Loose et al., 2017). Secondly, the assumption in model parametrizations that the simulated sea ice is impermeable to gas transfer has been challenged by observations (Gourdal et al., 2019). Thirdly, the biogeochemistry of marginal sea ice zones might not be accurately represented, especially in coarse resolution models, which could lead to an underestimation of DMS emissions. A recent study combining satellite remote sensing and field data estimated that north of 80°N, DMS emissions from the marginal ice zone are increasing and likely exceed open-water emissions in June and July (Galí et al., 2021). Considering the low resolution of CMIP6 models and their poor representation of small leads, Bock et al. (2021) conclude that CMIP6 models likely underestimate DMS emissions in ice-covered areas. The model analyzed here is of higher resolution than CMIP6 models and includes a nonlinear dependence of the DMS sea-to-air flux on sea ice concentration, with an enhancement of fluxes when sea ice concentrations are high. However, these extra features do not result in DMS emissions higher than all CMIP6 models, and instead the simulated time series of pan-Arctic means from CSIB-CanOE-NAA and CNRM-ESM2-1 are remarkably similar.

There is no consensus on the future trend of Arctic DMS concentrations, with CMIP6 models projecting both increases and decreases of the mean ocean surface DMS concentration. Two CMIP6 models have prognostic DMS cycles (NorESM2-LM, CNRM-ESM2-1) whereas the other two have diagnostic schemes, but these differences do not explain future trends, and each type of model simulates increases and decreases of ocean DMS concentrations. In their analysis of CMIP6 models, Bock et al. (2021) showed that DMS concentrations were strongly correlated to net primary production, similarly to the relationship found here between ocean surface DMS concentration and phytoplankton biomass. Therefore, the uncertainty in mean ocean surface DMS concentration can be linked to inter-model variability in the simulated trends for Arctic net primary production.

A source of uncertainty in future projections from climate models stems from scenario uncertainty, which can be assessed with simulations forced with different future emissions scenarios. Such an analysis has not been carried out for DMS production and emissions from CMIP6 models, but we have also run our model with the RCP4.5 scenario, corresponding to reduced emissions compared to RCP8.5. Comparison of pan-Arctic means shows that the increasing trends of future ocean surface DMS concentrations and DMS emissions are similar for both scenarios (Figure S8). Future projections from our model differ mainly in the timing when a given threshold is crossed, and for both variables considered here a given level reached by the simulation from RCP8.5 is attained by the simulation from RCP4.5 with a delay. This feature of climate model simulations is well documented for many variables; for example projections of Arctic sea ice area from various scenarios differ in the timing but not occurrence of sea-ice-free summers (Notz and Community, 2020). More generally, differences between projections from various emissions scenarios are reduced when considering a specific warming level rather than a specific time (Evin et al., 2024).

In contrast to CMIP6 models, the model analyzed here includes sea ice DMS production. The previous work from Hayashida et al. (2020) analyzing the CSIB-CanOE-NAA model simulations over the historical period found a substantial relative contribution of sea ice DMS to the overall production, especially during spring in regions of the high Arctic. Our analysis of future simulations shows that the contribution of sea ice DMS production could increase in the future, following trends of ice algal growth. Early in the 21st century, simulated reductions in sea ice thickness combined with small changes in the timing of sea ice break-up will result in the emergence of productive regions at high latitudes (Haddon et al., 2024). However, if the sea ice decline accelerates by the end of the 21st century, as projected by simulations with the high-end emission scenarios RCP8.5 and SSP585, some regions could see strong decreases in spring sea ice area, leading to loss of sea ice DMS production.

These uncertainties in DMS concentrations and emissions in the sea ice zone indicate that a better representation of sea ice processes is still needed to accurately simulate sulfur biogeochemistry in the Arctic. Likewise, Elliott et al. (2012) have also included ice algal DMS production in their model, noting difficulties and uncertainties in the development and evaluation of the sulfur biogeochemistry component due to the paucity of data for the Arctic. This paucity highlights the importance of detailed observations of both DMS emissions and the processes involved in the production and emissions of DMS to improve the representation of the sulfur cycle in models. Model simulations as the ones analyzed here can help identify regions of potential strong future changes, which could represent areas of focused observations to

understand the impacts of climate change on future S biogeochemistry. The southern Beaufort Sea and western Baffin Bay are projected to be among the first areas to lose a large portion of their sea ice DMS production; documenting such declines could provide insights on the consequences of sea ice loss. In contrast, the strongest increases in DMS emissions are simulated in the northern Barents Sea and the Chukchi Sea, such that these areas represent potential emerging hot-spots of interest.

4.2. Temporal variability of DMS emissions

4.2.1. Wind variability

The DMS emissions simulated by the CSIB-CanOE-NAA model are characterized by a strong temporal variability, with bursts of emissions that last a few days with high fluxes. The occurrence of short-term spikes in DMS emissions that are much greater than their monthly or seasonal averages implies that DMS can have an effect on atmospheric dynamics even in areas of low mean DMS emissions, albeit episodically.

The intermittency of DMS emissions highlights the necessity of using high-frequency data to capture the variability of DMS emissions and to fully account for the impact of DMS on the climate system. To the best of our knowledge, the strong temporal variability of DMS emissions has not been reported in previous 3D model studies, which could be due to the prevalence of analyzing model output with only monthly or seasonal averages. Furthermore, using a monthly climatology of DMS sea-to-air fluxes is insufficient to capture short bursts of DMS emissions and may lead to an inaccurate estimation of the role of DMS as a climate-active gas. A better alternative is to compute fluxes using a monthly climatology of ocean surface DMS concentrations in association with a daily surface wind speed data product. Such an approach, however, would neglect the strong spatio-temporal variability of DMS ocean concentrations from the patchiness of phytoplankton blooms, as discussed later.

Spikes of DMS emissions have been observed in polar regions (Trevena and Jones, 2012) and were documented as a regular feature during a 5-year study of a coastal area of the Western Antarctic Peninsula (Webb et al., 2019). Observations from Webb et al. (2019) resemble model simulations for the Eastern Arctic regions in the late 21st century, with the highest spikes during summer, when sea ice concentrations are between 10 and 40% and high levels of DMS have accumulated, potentially from ice algae and under-ice production. In observations and the model simulations presented here, the occurrence of these pulses require high ocean surface DMS concentrations, but the high frequency variability is the result of surface wind speeds variability. Such bursts of emissions occur also at lower latitudes, and high frequency sampling has shown a rapid and strong response of surface DMS concentrations to high wind events (Royer et al., 2016).

Simulated DMS emissions depend upon how fluxes are parameterized. Recent observations have found a reduction of DMS emissions for instantaneous wind speeds greater than 11 m s^{-1}, resulting from the interactions between waves and wind (Zavarsky et al., 2018). In contrast, a study focusing on high wind speeds found that gas transfer velocities for DMS were not suppressed significantly by large waves (Blomquist et al., 2017). Furthermore, the quadratic wind speed parametrization from Nightingale et al. (2000) has been challenged by a number of studies (Marandino et al., 2007; Blomquist et al., 2017; Zavarsky et al., 2018; Fairall et al., 2022). Comparing the gas transfer velocity used in our model (k_{N00}; Nightingale et al., 2000) with a linear wind speed parametrization (k_{Z18}; Zavarsky et al., 2018) shows that for wind speeds lower than 8 m s^{-1} the gas transfer velocities are close, with k_{Z18} slightly higher than k_{N00} (Figure S9). For higher wind speeds, however, k_{N00} parametrization gives a much stronger gas transfer velocity than k_{Z18}. To assess the impact of the choice of parametrization on our results, we compared May and August climatological means from DMS emissions re-computed with both parametrizations (Figures S10 and S11). This analysis revealed that the k_{Z18} parametrization would lead to higher average DMS emissions but unchanged spatial patterns, which is expected as daily mean wind speeds rarely exceed 10 m s^{-1} during summer when DMS production occurs in the Arctic (**Figure 7**). The choice of gas transfer velocity parametrization could also impact the temporal variability of DMS sea-to-air fluxes due to the strong influence of wind variability on DMS emissions intermittency, but the temporal distributions of daily DMS sea-to-air fluxes with both parametrizations are similar (Figures S12 and S13). With the linear wind speed dependence of k_{Z18}, there are still substantial spikes of DMS emissions, and their occurrence is not strongly reduced. This analysis suggests that our results would hold qualitatively with a linear wind speed parametrization, but a focused study with different sea-to-air flux parametrizations would be necessary for a quantitative assessment of the uncertainty associated with the choice of parametrization. Such a sensitivity analysis is still lacking, in particular in a polar context where it is necessary to take into account the complex interactions between the ocean, sea ice and wind.

While wind clearly plays a central role in the variability and magnitude of sea-to-air fluxes, it impacts DMS emissions in a variety of other ways. Wind-driven mixing influences the mixed layer depth and can therefore affect ocean DMS concentrations, as will be discussed later. In particular, rapid changes of the MLD have been shown to impact the temporal variability of DMS concentrations and emissions (Steiner et al., 2012).

The future of DMS emissions will depend strongly on how climate change affects wind. In the simulations presented here, both mean DMS emissions and the frequency of high DMS emissions increase from present to late 21st century. These changes can be linked to increases in mean wind speeds and greater occurrence of strong wind events. Both CMIP5 and regional models also project increases in monthly mean and monthly averages of daily maximum wind speeds, throughout the Arctic for both RCP4.5 and RCP8.5 scenarios (Reader and Steiner, 2022). A major factor influencing surface wind speeds in polar regions is the sea ice cover, as it impacts surface roughness, with the presence of sea ice leading to lower near-surface wind

speeds. The substantial loss of sea ice during summer is therefore expected to result in increases in mean wind speeds. Projecting the future of wind speed distributions and in particular the frequency of high wind speed events is much less straightforward. There is a high degree of uncertainty in future changes in atmospheric dynamics affecting wind, as a number of interdependent atmospheric processes could be impacted in a variety of manners by climate change (Reader and Steiner, 2022; Ruman et al., 2022; Miyawaki et al., 2023). For example, a particular feature of high latitude regions are polar lows, which are intense maritime mesoscale weather systems lasting less than 3 days that can lead to high DMS emissions events. However, until recently the resolution of atmospheric models was too coarse to reproduce polar lows accurately, and there is still a high uncertainty on the future of these storms and how they will be impacted by climate change (Moreno-Ibáñez et al., 2021).

The strong impact of wind on DMS emissions also raises the issue of the dependence of simulations on the atmospheric forcing used for ocean models. Here in particular, the forcing used has a 25 km resolution, and therefore small-scale wind patterns are not represented, causing an underestimation of the spatial variability of wind and thus of DMS emissions (Bessac et al., 2019).

4.2.2. Sea ice processes

Field studies in the sea ice zone have reported short but strong out-gassing events as sea ice starts to break-up, when DMS trapped in and below sea ice can be vented to the atmosphere through the first narrow leads (Trevena and Jones, 2012). This process represents another form of temporal variability, controlled by sea ice dynamics at a small scale. However, the model used here does not simulate these out-gassing events that occur at the onset of sea ice break-up. The current model resolution and the absence of a sub-grid representation of leads clearly limits the ability to reproduce such bursts of DMS emissions. In addition, despite the simulated accumulation of high concentrations of DMS in sea ice, the model does not represent direct emission from sea ice to the atmosphere. Instead, DMS produced by ice algae must first be released to the ocean surface layer, where it is diluted due to the large thickness difference between the ice skeletal layer and ocean surface layer (3 cm versus 1 m). This dilution results in ocean surface DMS concentrations lower than in sea ice, which strongly reduces the potential for high DMS emissions from ice algal production.

The relation between sea ice concentration and DMS emissions is more complex than the linear relation suggested by both our model and CMIP6 models. Sea ice dynamics and mechanisms controlling leads will have an impact on the magnitude and timing of future DMS emissions, and thus an improved representation of small-scale features of sea ice are also necessary to make accurate projections of the future sulfur cycle in polar regions. In particular, these model improvements would allow a better reproduction of pulses of DMS emissions, which are disproportionately important to climate-relevant processes.

4.3. Spatial variability of DMS concentrations

In both sea ice and the ocean, a strong linear relationship between DMS concentrations and the biomass of primary producers was found in model simulations. However, this relationship varies in time and space, indicating that the link between phytoplankton and DMS is not based on a simple uniform multiplicative factor. Statistical relationships have also been identified in observational datasets of chlorophyll or environmental variables, such as solar irradiance (Yang et al., 1999; Vallina and Simó, 2007). While these relationships have been found to hold even globally, data in these studies were binned over large areas, for example, by averaging in 10° latitude by 20° longitude boxes. A later study re-examining the relationship between DMS concentrations and solar irradiance with less spatial aggregation found very little correlation, indicating that other factors influence DMS production (Derevianko et al., 2009). Using an artificial neural network, Wang et al. (2020) have succeeded in explaining 66% of the variance in the DMS concentration data with a variety of environmental variables and with minimal spatial aggregation. This result highlights the complexity and nonlinearity between DMS production and factors that influence it. The variability of the phytoplankton-DMS relationship is the result of the various processes involved in DMS production but is also impacted by phytoplankton taxonomy, as different groups of primary producers have different DMS production capabilities (Stefels et al., 2007). The representation of this relationship is thus influenced by the choice of parametrizations and the level of detail of the phytoplankton model. As a result, the phytoplankton-DMS relationship is a further source of uncertainty that could strongly impact future projections of the Arctic sulfur biogeochemistry.

Our model simulates substantial spatial variability of DMS concentrations. Field studies have linked observed variability of DMS production at different scales to phytoplankton community composition, as different groups of phytoplankton have different DMS production capabilities (Luce et al., 2011; Steiner et al., 2012; Park et al., 2018). Another source of variability at sub-mesoscales is the patchiness of phytoplankton blooms, which remains poorly represented in models due to insufficient resolution (Martin, 2003), indicating that there is likely more spatial variability in DMS concentrations and emissions than simulated in the model presented here.

The simulated DMS production takes place in the upper ocean, with substantial production below the MLD during summer. Such deep production has been observed routinely at lower latitudes, when a deep chlorophyll maximum develops (Bailey et al., 2008; Galí et al., 2013; Royer et al., 2016). The model used here has been shown to have a low biased subsurface chlorophyll maximum (Steiner et al., 2024), and thus our simulations could underestimate concentrations below the MLD. At lower latitudes, the upward transport through mixing of DMS produced below the MLD has been estimated from observational data, showing that it is negligible compared to other fluxes, such as bacterial consumption (Galí et al., 2013; Yang et al., 2013). However, Royer et al. (2016) have shown that strong wind events can lead to a temporary increase in mixing and result in deep DMS being supplied to the surface layers, thereby contributing

to emissions. Detecting such events requires a high temporal resolution, which remains impractical for long simulation of 3D ocean models as we analyze here. Nonetheless, from the monthly means available for this study, the majority of deep DMS production appears to remain trapped under the MLD and does not contribute to emissions, being degraded instead at depth by bacterial consumption.

Potential changes in ocean mixing will also affect DMS concentrations and emissions later in the 21st century. Stratification is projected to increase in the Arctic Ocean, which is expected to reduce nutrient availability for primary production. However, these effects could be offset by increased light availability from sea ice loss, and there is still a high degree of uncertainty in the future of primary production as projected by global models (Vancoppenolle et al., 2013; Noh et al., 2023). Vertical mixing also impacts DMS concentrations, as it has an effect on phytoplankton taxonomy and physiology (Stefels et al., 2007) as well as their exposure to light (Vallina and Simó, 2007). Changes in the MLD affect the ultraviolet radiation exposure of DMS-consuming bacteria, which has been shown to impact DMS concentrations sufficiently to explain the relationship between MLD and DMS concentrations (Simó and Pedrós-Alió, 1999; Steiner et al., 2006; Toole et al., 2006).

5. Conclusions

Using a regional ocean and sea ice biogeochemical model of the Arctic, the future of DMS concentrations and emissions has been analyzed in this work. Three groups of regions were identified:

- Eastern Arctic: Chukchi, East Siberian, Laptev, and Kara seas. The loss of a summer sea ice cover in these regions results in earlier and increased DMS emissions from the removal of a physical barrier. On these shallow continental shelves, simulated DMS production and primary production are also earlier and larger by the late 21st century. These changes are the consequence of greater light and nutrient availability, as thinner sea ice year-round allows for more light and momentum transfer to the ocean.
- Central and Western Arctic: Central Arctic, Beaufort Sea, Canadian Arctic Archipelago, and Baffin Bay. In these regions, spring DMS production remains trapped below sea ice even in the late 21st century, as small changes in spring sea ice concentrations are simulated. In summer, despite strong sea ice loss, DMS production occurs mostly below the mixed layer depth and does not contribute to DMS emissions.
- Atlantic Arctic: Barents and GIN seas. These regions are already mostly sea-ice-free in the present, hence projected changes in the sulfur biogeochemistry are small. Nonetheless, increases in the occurrence of high wind speed events lead to a simulated increase of the frequency of high DMS emissions bursts.

We have identified the following key mechanisms governing Arctic DMS, and how these will be impacted by climate change:

1. Wind variability induces a strong short-term temporal variability of DMS emissions. Substantial bursts of DMS emissions are simulated throughout the Arctic, including in areas of low DMS emissions, indicating the possibility of an impact of DMS on climate even in the Central Arctic and other regions of low mean DMS concentrations.
2. Despite increasing DMS concentrations from ice algal and under-ice blooms, the model does not simulate DMS out-gassing events during sea ice break-up. Better representation of leads and higher model resolution are still necessary to capture bursts of DMS emissions during sea ice break-up.
3. Substantial quantities of DMS are produced at depth when a deep chlorophyll maximum develops. During summer, when the MLD is shallow, this DMS remains trapped at depth, below the mixed layer and does not contribute to emissions.

This work highlights the key role that sea ice and wind play in controlling DMS emissions in the Arctic. These variables are also drivers of ocean DMS concentrations through their control of light and nutrient availability, which regulate the primary producers responsible for DMS production. While future work should focus on improving the representation of these physical drivers, developments toward a more detailed modeling of S biogeochemistry are also still required. Notably, methanetiol (MeSH) is another sulfur aerosol precursor produced in substantial amounts in the ocean and sea ice, with recent evidence suggesting that emissions of MeSH are particularly strong in polar oceans (Wohl et al., 2024). Production and emission of this compound should be added to sulfur biogeochemical models, especially considering that it is also a product of the degradation of DMSP and thus represents only a minor increase of model complexity.

Data accessibility statement

The model code and the configuration used for model simulations are archived in the repository Hayashida (2020) (https://zenodo.org/doi/10.5281/zenodo.3697355). The processed model output data analyzed here are archived in the repository Haddon et al. (2025) (https://doi.org/10.5281/zenodo.15299390). Full model output is hosted on Digital Research Alliance of Canada infrastructures and can be made available upon request. Scripts for the analysis of model output are archived in the repository Haddon (2023) (https://zenodo.org/doi/10.5281/zenodo.10045060.)

Supplemental files

The supplemental files for this article can be found as follows:

- Figure S1: RMSE in recomputing daily DMS emissions
- Figure S2: Mean biases in recomputing daily DMS emissions
- Figure S3: Coefficient of determination of ocean surface DMS and phytoplankton relation.

- Figure S4: Annual cycles of vertical profiles of the Central and Western Arctic.
- Figure S5: Annual cycles of vertical profiles of the Eastern Arctic.
- Figure S6: Annual cycles of vertical profiles of the Atlantic Arctic.
- Figure S7: May mixed layer total DMS.
- Figure S8: Comparison of RCP4.5 and RCP8.5 scenarios.
- Figure S9: Comparison of DMS flux parametrizations.
- Figure S10: Comparison of present mean DMS emissions for different sea-to-air DMS flux parametrizations.
- Figure S11: Comparison of late 21st century mean DMS emissions for different sea-to-air DMS flux parametrizations.
- Figure S12: Comparison of temporal distributions of present DMS emissions for different sea-to-air DMS flux parametrizations.
- Figure S13: Comparison of temporal distributions of late 21st century DMS emissions for different sea-to-air DMS flux parametrizations.

Acknowledgment

The authors acknowledge constructive discussions within the Institute of Ocean Sciences and Canadian Center for Climate Modelling and Analysis biogeochemical modelling working group. This research was enabled in part by support provided by BC DRI Group and the Digital Research Alliance of Canada (https://alliancecan.ca).

Funding

This project has received funding from the National Science and Engineering Council of Canada New Frontiers in Research Fund (NSERC-NFRFG-2020-00451) in association with the European Union's Horizon 2020 research and innovation program under grant agreement No 101003826 via project CRiceS (Climate Relevant interactions and feedbacks: the key role of sea ice and Snow in the polar and global climate system). NS and TS acknowledge funding through Fisheries and Oceans Canada. This work contributes to BEPSII (Biogeochemical Exchange Processes at Sea Ice Interfaces) and the Surface Ocean-Lower Atmosphere Study (SOLAS), which is partially supported by the U.S. National Science Foundation (Grant OCE-2140395) via the Scientific Committee on Oceanic Research (SCOR). This work also contributes to Cice2-Clouds which is supported with NSF grant number OCE-2140395.

Competing interests

Authors have no competing interests to declare.

Author contributions

- Substantial contributions to conception and design: AH, AHM, NS.
- Acquisition of data: AH, TS.
- Analysis and interpretation of data: AH, AHM, NS.
- Drafting the article or revising it critically for important intellectual content: All authors.
- Final approval of the version to be published: All authors.

References

Abbatt, JPD, **Leaitch, WR**, **Aliabadi, AA**, **Bertram, AK**, **Blanchet, JP**, **Boivin-Rioux, A**, **Bozem, H**, **Burkart, J**, **Chang, RYW**, **Charette, J**, **Chaubey, JP**, **Christensen, RJ**, **Cirisan, A**, **Collins, DB**, **Croft, B**, **Dionne, J**, **Evans, GJ**, **Fletcher, CG**, **Galí, M**, **Ghahreman, R**, **Girard, E**, **Gong, W**, **Gosselin, M**, **Gourdal, M**, **Hanna, SJ**, **Hayashida, H**, **Herber, AB**, **Hesaraki, S**, **Hoor, P**, **Huang, L**, **Hussherr, R**, **Irish, VE**, **Keita, SA**, **Kodros, JK**, **Köllner, F**, **Kolonjari, F**, **Kunkel, D**, **Ladino, LA**, **Law, K**, **Levasseur, M**, **Libois, Q**, **Liggio, J**, **Lizotte, M**, **Macdonald, KM**, **Mahmood, R**, **Martin, RV**, **Mason, RH**, **Miller, LA**, **Moravek, A**, **Mortenson, E**, **Mungall, EL**, **Murphy, JG**, **Namazi, M**, **Norman, AL**, **O'Neill, NT**, **Pierce, JR**, **Russell, LM**, **Schneider, J**, **Schulz, H**, **Sharma, S**, **Si, M**, **Staebler, RM**, **Steiner, NS**, **Thomas, JL**, **von Salzen, K**, **Wentzell, JJB**, **Willis, MD**, **Wentworth, GR**, **Xu, JW**, **Yakobi-Hancock, JD.** 2019. Overview paper: New insights into aerosol and climate in the Arctic. *Atmospheric Chemistry and Physics* **19**(4): 2527–2560. DOI: http://dx.doi.org/10.5194/acp-19-2527-2019.

Andreae, MO, **Raemdonck, H.** 1983. Dimethyl sulfide in the surface ocean and the marine atmosphere: A global view. *Science* **221**(4612): 744–747. DOI: http://dx.doi.org/10.1126/science.221.4612.744.

Arora, VK, **Scinocca, JF**, **Boer, GJ**, **Christian, JR**, **Denman, KL**, **Flato, GM**, **Kharin, VV**, **Lee, WG**, **Merryfield, WJ.** 2011. Carbon emission limits required to satisfy future representative concentration pathways of greenhouse gases. *Geophysical Research Letters* **38**(5). DOI: http://dx.doi.org/10.1029/2010GL046270.

Bailey, KE, **Toole, DA**, **Blomquist, B**, **Najjar, RG**, **Huebert, B**, **Kieber, DJ**, **Kiene, RP**, **Matrai, P**, **Westby, GR**, **del Valle, DA.** 2008. Dimethylsulfide production in Sargasso Sea eddies. *Deep Sea Research Part II: Topical Studies in Oceanography* **55**(10–13): 1491–1504. DOI: http://dx.doi.org/10.1016/j.dsr2.2008.02.011.

Bates, TS, **Lamb, BK**, **Guenther, A**, **Dignon, J**, **Stoiber, RE.** 1992. Sulfur emissions to the atmosphere from natural sourees. *Journal of Atmospheric Chemistry* **14**(1): 315–337. DOI: http://dx.doi.org/10.1007/BF00115242.

Bessac, J, **Monahan, AH**, **Christensen, HM**, **Weitzel, N.** 2019. Stochastic parameterization of subgrid-scale velocity enhancement of sea surface fluxes. *Monthly Weather Review* **147**(5): 1447–1469. DOI: http://dx.doi.org/10.1175/MWR-D-18-0384.1.

Blomquist, BW, **Brumer, SE**, **Fairall, CW**, **Huebert, BJ**, **Zappa, CJ**, **Brooks, IM**, **Yang, M**, **Bariteau, L**, **Prytherch, J**, **Hare, JE**, **Czerski, H**, **Matei, A**,

Pascal, RW. 2017. Wind speed and sea state dependencies of air-sea gas transfer: Results from the high wind speed gas exchange study (HiWinGS). *Journal of Geophysical Research: Oceans* **122**(10): 8034–8062. DOI: http://dx.doi.org/10.1002/2017JC013181.

Bock, J, **Michou, M**, **Nabat, P**, **Abe, M**, **Mulcahy, JP**, **Olivié, DJL**, **Schwinger, J**, **Suntharalingam, P**, **Tjiputra, J**, **van Hulten, M**, **Watanabe, M**, **Yool, A**, **Séférian, R.** 2021. Evaluation of ocean dimethylsulfide concentration and emission in CMIP6 models. *Biogeosciences* **18**(12): 3823–3860. DOI: http://dx.doi.org/10.5194/bg-18-3823-2021.

Bouillon, S, **Morales Maqueda, MÁ**, **Legat, V**, **Fichefet, T.** 2009. An elastic–viscous–plastic sea ice model formulated on Arakawa B and C grids. *Ocean Modelling* **27**(3–4): 174–184. DOI: http://dx.doi.org/10.1016/j.ocemod.2009.01.004.

Bullock, HA, **Luo, H**, **Whitman, WB.** 2017. Evolution of dimethylsulfoniopropionate metabolism in marine phytoplankton and bacteria. *Frontiers in Microbiology* **8**: 637. DOI: http://dx.doi.org/10.3389/fmicb.2017.00637.

Campen, HI, **Arévalo-Martínez, DL**, **Artioli, Y**, **Brown, IJ**, **Kitidis, V**, **Lessin, G**, **Rees, AP**, **Bange, HW.** 2022. The role of a changing Arctic Ocean and climate for the biogeochemical cycling of dimethyl sulphide and carbon monoxide. *Ambio* **51**(2): 411–422. DOI: http://dx.doi.org/10.1007/s13280-021-01612-z.

Christian, JR, **Denman, KL**, **Hayashida, H**, **Holdsworth, AM**, **Lee, WG**, **Riche, OGJ**, **Shao, AE**, **Steiner, N**, **Swart, NC.** 2022. Ocean biogeochemistry in the Canadian Earth System Model Version 5.0.3: CanESM5 and CanESM5-CanOE. *Geoscientific Model Development* **15**(11): 4393–4424. DOI: http://dx.doi.org/10.5194/gmd-15-4393-2022.

Derevianko, GJ, **Deutsch, C**, **Hall, A.** 2009. On the relationship between ocean DMS and solar radiation. *Geophysical Research Letters* **36**(17). DOI: http://dx.doi.org/10.1029/2009GL039412.

Elliott, S, **Deal, C**, **Humphries, G**, **Hunke, E**, **Jeffery, N**, **Jin, M**, **Levasseur, M**, **Stefels, J.** 2012. Pan-Arctic simulation of coupled nutrient-sulfur cycling due to sea ice biology: Preliminary results. *Journal of Geophysical Research: Biogeosciences* **117**(G1). DOI: http://dx.doi.org/10.1029/2011JG001649.

Evin, G, **Ribes, A**, **Corre, L.** 2024. Assessing CMIP6 uncertainties at global warming levels. *Climate Dynamics* **62**(8): 8057–8072. DOI: http://dx.doi.org/10.1007/s00382-024-07323-x.

Fairall, CW, **Yang, M**, **Brumer, SE**, **Blomquist, BW**, **Edson, JB**, **Zappa, CJ**, **Bariteau, L**, **Pezoa, S**, **Bell, TG**, **Saltzman, ES.** 2022. Air-sea trace gas fluxes: Direct and indirect measurements. *Frontiers in Marine Science* **9**: 826606. DOI: http://dx.doi.org/10.3389/fmars.2022.826606.

Gabric, A, **Gregg, W**, **Najjar, R**, **Erickson, D**, **Matrai, P.** 2001. Modeling the biogeochemical cycle of dimethylsulfide in the upper ocean: A review. *Chemosphere - Global Change Science* **3**(4): 377–392. DOI: http://dx.doi.org/10.1016/S1465-9972(01)00018-6.

Gabric, AJ, **Qu, B**, **Matrai, P**, **Hirst, AC.** 2005. The simulated response of dimethylsulfide production in the Arctic Ocean to global warming. *Tellus B: Chemical and Physical Meteorology* **57**(5): 391–403. DOI: https://doi.org/10.3402/tellusb.v57i5.16564.

Galí, M, **Devred, E**, **Babin, M**, **Levasseur, M.** 2019. Decadal increase in Arctic dimethylsulfide emission. *Proceedings of the National Academy of Sciences* **116**(39): 19311–19317. DOI: http://dx.doi.org/10.1073/pnas.1904378116.

Galí, M, **Lizotte, M**, **Kieber, DJ**, **Randelhoff, A**, **Hussherr, R**, **Xue, L**, **Dinasquet, J**, **Babin, M**, **Rehm, E**, **Levasseur, M.** 2021. DMS emissions from the Arctic marginal ice zone. *Elementa: Science of the Anthropocene* **9**(1): 00113. DOI: http://dx.doi.org/10.1525/elementa.2020.00113.

Galí, M, **Simó, R**, **Vila-Costa, M**, **Ruiz-González, C**, **Gasol, JM**, **Matrai, P.** 2013. Diel patterns of oceanic dimethylsulfide (DMS) cycling: Microbial and physical drivers. *Global Biogeochemical Cycles* **27**(3): 620–636. DOI: http://dx.doi.org/10.1002/gbc.20047.

Gourdal, M, **Crabeck, O**, **Lizotte, M**, **Galindo, V**, **Gosselin, M**, **Babin, M**, **Scarratt, M**, **Levasseur, M.** 2019. Upward transport of bottom-ice dimethyl sulfide during advanced melting of arctic first-year sea ice. *Elementa: Science of the Anthropocene* **7**: 33. DOI: http://dx.doi.org/10.1525/elementa.370.

Haddon, A. 2023. Scripts for the analysis of CSIB model output: V2023.10.26. Zenodo. DOI: http://dx.doi.org/10.5281/zenodo.10045061.

Haddon, A, **Farnole, P**, **Monahan, AH**, **Sou, T**, **Steiner, N.** 2024. Environmental controls and phenology of sea ice algal growth in a future Arctic. *Elementa: Science of the Anthropocene* **12**(1): 00129. DOI: http://dx.doi.org/10.1525/elementa.2023.00129.

Haddon, A, **Steiner, N**, **Sou, T**, **Monahan, A.** 2025. CSIB model output: DMS and sea ice algal biomass. Zenodo. DOI: http://dx.doi.org/10.5281/zenodo.15299391.

Hayashida, H. 2020. Model code and output of CSIBv4 pan-Arctic sea ice-ocean DMS simulation. Zenodo. DOI: http://dx.doi.org/10.5281/zenodo.3697356.

Hayashida, H, **Carnat, G**, **Galí, M**, **Monahan, AH**, **Mortenson, E**, **Sou, T**, **Steiner, NS.** 2020. Spatio-temporal variability in modeled bottom ice and sea surface dimethylsulfide concentrations and fluxes in the arctic during 1979–2015. *Global Biogeochemical Cycles* **34**(10): e2019GB006456. DOI: http://dx.doi.org/10.1029/2019GB006456.

Hayashida, H, **Christian, JR**, **Holdsworth, AM**, **Hu, X**, **Monahan, AH**, **Mortenson, E**, **Myers, PG**, **Riche, OGJ**, **Sou, T**, **Steiner, NS.** 2019. CSIB v1 (Canadian Sea-ice Biogeochemistry): A sea-ice biogeochemical model for the NEMO community ocean modelling framework. *Geoscientific Model Development* **12**(5):

1965–1990. DOI: http://dx.doi.org/10.5194/gmd-12-1965-2019.

Hayashida, H, **Steiner, N**, **Monahan, A**, **Galindo, V**, **Lizotte, M**, **Levasseur, M.** 2017. Implications of sea-ice biogeochemistry for oceanic production and emissions of dimethyl sulfide in the Arctic. *Biogeosciences* **14**(12): 3129–3155. DOI: http://dx.doi.org/10.5194/bg-14-3129-2017.

Hu, X, **Myers, PG.** 2013. A Lagrangian view of Pacific water inflow pathways in the Arctic Ocean during model spin-up. *Ocean Modelling* **71**: 66–80. DOI: http://dx.doi.org/10.1016/j.ocemod.2013.06.007.

Hulswar, S, **Simó, R**, **Galí, M**, **Bell, TG**, **Lana, A**, **Inamdar, S**, **Halloran, PR**, **Manville, G**, **Mahajan, AS.** 2022. Third revision of the global surface seawater dimethyl sulfide climatology (DMS-Rev3). *Earth System Science Data* **14**(7): 2963–2987. DOI: http://dx.doi.org/10.5194/essd-14-2963-2022.

IPCC. 2021. *Climate change 2021 – The physical science basis: Working group i contribution to the sixth assessment report of the Intergovernmental Panel on Climate Change*. Cambridge, UK: Cambridge University Press. DOI: http://dx.doi.org/10.1017/9781009157896.

Jodwalis, CM, **Benner, RL**, **Eslinger, DL.** 2000. Modeling of dimethyl sulfide ocean mixing, biological production, and sea-to-air flux for high latitudes. *Journal of Geophysical Research: Atmospheres* **105**(D11): 14387–14399. DOI: http://dx.doi.org/10.1029/2000JD900023.

Kloster, S, **Six, KD**, **Feichter, J**, **Maier-Reimer, E**, **Roeckner, E**, **Wetzel, P**, **Stier, P**, **Esch, M.** 2007. Response of dimethylsulfide (DMS) in the ocean and atmosphere to global warming. *Journal of Geophysical Research: Biogeosciences* **112**(G3). DOI: http://dx.doi.org/10.1029/2006JG000224.

Levasseur, M. 2013. Impact of Arctic meltdown on the microbial cycling of sulphur. *Nature Geoscience* **6**(9): 691–700. DOI: http://dx.doi.org/10.1038/ngeo1910.

Loose, B, **Kelly, RP**, **Bigdeli, A**, **Williams, W**, **Krishfield, R**, **Rutgers van der Loeff, M**, **Moran, SB.** 2017. How well does wind speed predict air-sea gas transfer in the sea ice zone? A synthesis of radon deficit profiles in the upper water column of the Arctic Ocean. *Journal of Geophysical Research: Oceans* **122**(5): 3696–3714. DOI: http://dx.doi.org/10.1002/2016JC012460.

Loose, B, **McGillis, WR**, **Schlosser, P**, **Perovich, D**, **Takahashi, T.** 2009. Effects of freezing, growth, and ice cover on gas transport processes in laboratory seawater experiments. *Geophysical Research Letters* **36**(5). DOI: http://dx.doi.org/10.1029/2008GL036318.

Luce, M, **Levasseur, M**, **Scarratt, MG**, **Michaud, S**, **Royer, S-J**, **Kiene, R**, **Lovejoy, C**, **Gosselin, M**, **Poulin, M**, **Gratton, Y**, **Lizotte, M.** 2011. Distribution and microbial metabolism of dimethylsulfoniopropionate and dimethylsulfide during the 2007 Arctic ice minimum. *Journal of Geophysical Research: Oceans* **116**(C9). DOI: http://dx.doi.org/10.1029/2010JC006914.

Madec, G, **Bourdallé-Badie, R**, **Bouttier, PA**, **Bricaud, C**, **Bruciaferri, D**, **Calvert, D**, **Chanut, J**, **Clementi, E**, **Coward, A**, **Delrosso, D**, **Ethé, C**, **Flavoni, S**, **Graham, T**, **Harle, J**, **Iovino, D**, **Lea, D**, **Lévy, C**, **Lovato, T**, **Martin, N**, **Masson, S**, **Mocavero, S**, **Paul, J**, **Rousset, C**, **Storkey, D**, **Storto, A**, **Vancoppenolle, M.** 2017. NEMO ocean engine. IPSL. DOI: http://dx.doi.org/10.5281/zenodo.3248739.

Marandino, CA, **De Bruyn, WJ**, **Miller, SD**, **Saltzman, ES.** 2007. Eddy correlation measurements of the air/sea flux of dimethylsulfide over the North Pacific Ocean. *Journal of Geophysical Research: Atmospheres* **112**(D3). DOI: http://dx.doi.org/10.1029/2006JD007293.

Martin, AP. 2003. Phytoplankton patchiness: The role of lateral stirring and mixing. *Progress in Oceanography* **57**(2): 125–174. DOI: http://dx.doi.org/10.1016/S0079-6611(03)00085-5.

Matrai, P, **Apollonio, S.** 2013. New estimates of microalgae production based upon nitrate reductions under sea ice in Canadian shelf seas and the Canada Basin of the Arctic Ocean. *Marine Biology* **160**(6): 1297–1309. DOI: http://dx.doi.org/10.1007/s00227-013-2181-0.

Miyawaki, O, **Shaw, TA**, **Jansen, MF.** 2023. The emergence of a new wintertime Arctic energy balance regime. *Environmental Research: Climate* **2**(3): 031003. DOI: http://dx.doi.org/10.1088/2752-5295/aced63.

Moffett, CE, **Barrett, TE**, **Liu, J**, **Gunsch, MJ**, **Upchurch, LM**, **Quinn, PK**, **Pratt, KA**, **Sheesley, RJ.** 2020. Long-term trends for marine sulfur aerosol in the alaskan arctic and relationships with temperature. *Journal of Geophysical Research: Atmospheres* **125**(22): e2020JD033225. DOI: http://dx.doi.org/10.1029/2020JD033225.

Moreno-Ibáñez, M, **Laprise, R**, **Gachon, P.** 2021. Recent advances in polar low research: Current knowledge, challenges and future perspectives. *Tellus A: Dynamic Meteorology and Oceanography* **73**(1): 1–31. DOI: http://dx.doi.org/10.1080/16000870.2021.1890412.

Mortenson, E, **Hayashida, H**, **Steiner, N**, **Monahan, A**, **Blais, M**, **Gale, MA**, **Galindo, V**, **Gosselin, M**, **Hu, X**, **Lavoie, D**, **Mundy, CJ.** 2017. A model-based analysis of physical and biological controls on ice algal and pelagic primary production in Resolute Passage. *Elementa: Science of the Anthropocene* **5**: 39. DOI: http://dx.doi.org/10.1525/elementa.229.

Nightingale, PD, **Malin, G**, **Law, CS**, **Watson, AJ**, **Liss, PS**, **Liddicoat, MI**, **Boutin, J**, **Upstill-Goddard, RC.** 2000. In situ evaluation of air-sea gas exchange parameterizations using novel conservative and volatile tracers. *Global Biogeochemical Cycles* **14**(1): 373–387. DOI: http://dx.doi.org/10.1029/1999GB900091.

Noh, KM, **Lim, H-G**, **Yang, EJ**, **Kug, J-S.** 2023. Emergent constraint for future decline in Arctic phytoplankton

concentration. *Earth's Future* **11**(4): e2022EF003427. DOI: http://dx.doi.org/10.1029/2022EF003427.

Notz, D, **Community, S.** 2020. Arctic sea ice in CMIP6. *Geophysical Research Letters* **47**(10): e2019GL086749. DOI: http://dx.doi.org/10.1029/2019GL086749.

Pandis, SN, **Russell, LM**, **Seinfeld, JH.** 1994. The relationship between DMS flux and CCN concentration in remote marine regions. *Journal of Geophysical Research: Atmospheres* **99**(D8): 16945–16957. DOI: http://dx.doi.org/10.1029/94JD01119.

Park, K-T, **Jang, S**, **Lee, K**, **Yoon, YJ**, **Kim, M-S**, **Park, K**, **Cho, H-J**, **Kang, J-H**, **Udisti, R**, **Lee, B-Y**, **Shin, K-H.** 2017. Observational evidence for the formation of DMS-derived aerosols during Arctic phytoplankton blooms. *Atmospheric Chemistry and Physics* **17**(15): 9665–9675. DOI: http://dx.doi.org/10.5194/acp-17-9665-2017.

Park, K-T, **Lee, K**, **Kim, T-W**, **Yoon, YJ**, **Jang, E-H**, **Jang, S**, **Lee, B-Y**, **Hermansen, O.** 2018. Atmospheric DMS in the arctic ocean and its relation to phytoplankton biomass. *Global Biogeochemical Cycles* **32**(3): 351–359. DOI: http://dx.doi.org/10.1002/2017GB005805.

Park, K-T, **Yoon, YJ**, **Lee, K**, **Tunved, P**, **Krejci, R**, **Ström, J**, **Jang, E**, **Kang, HJ**, **Jang, S**, **Park, J**, **Lee, BY**, **Traversi, R**, **Becagli, S**, **Hermansen, O.** 2021. Dimethyl sulfide-induced increase in cloud condensation nuclei in the arctic atmosphere. *Global Biogeochemical Cycles* **35**(7): e2021GB006969. DOI: http://dx.doi.org/10.1029/2021GB006969.

Reader, MC, **Steiner, N.** 2022. Atmospheric trends over the Arctic Ocean in simulations from the coordinated regional downscaling experiment (CORDEX) and their driving GCMs. *Climate Dynamics* **59**(11): 3401–3426. DOI: http://dx.doi.org/10.1007/s00382-022-06274-5.

Royer, S-J, **Galí, M**, **Mahajan, AS**, **Ross, ON**, **Pérez, GL**, **Saltzman, ES**, **Simó, R.** 2016. A high-resolution time-depth view of dimethylsulphide cycling in the surface sea. *Scientific Reports* **6**(1): 32325. DOI: http://dx.doi.org/10.1038/srep32325.

Ruman, CJ, **Monahan, AH**, **Sushama, L.** 2022. Climatology of Arctic temperature inversions in current and future climates. *Theoretical and Applied Climatology* **150**(1): 121–134. DOI: http://dx.doi.org/10.1007/s00704-022-04147-9.

Saltzman, ES, **King, DB**, **Holmen, K**, **Leck, C.** 1993. Experimental determination of the diffusion coefficient of dimethylsulfide in water. *Journal of Geophysical Research: Oceans* **98**(C9): 16481–16486. DOI: http://dx.doi.org/10.1029/93JC01858.

Sellegri, K, **Simó, R**, **Wang, B**, **Alpert, PA**, **Altieri, K**, **Burrows, S**, **Hopkins, FE**, **Koren, I**, **McCoy, IL**, **Ovadnevaite, J**, **Salter, M**, **Schmale, J.** 2024. Influence of open ocean biogeochemistry on aerosol and clouds: Recent findings and perspectives. *Elementa: Science of the Anthropocene* **12**(1): 00058. DOI: http://dx.doi.org/10.1525/elementa.2023.00058.

Simó, R, **Pedrós-Alió, C.** 1999. Role of vertical mixing in controlling the oceanic production of dimethyl sulphide. *Nature* **402**(6760): 396–399. DOI: http://dx.doi.org/10.1038/46516.

Stefels, J, **Steinke, M**, **Turner, S**, **Malin, G**, **Belviso, S.** 2007. Environmental constraints on the production and removal of the climatically active gas dimethylsulphide (DMS) and implications for ecosystem modelling. *Biogeochemistry* **83**(1): 245–275. DOI: http://dx.doi.org/10.1007/s10533-007-9091-5.

Steiner, N, **Christian, J**, **Riche, O**, **Sou, T.** 2024. *Arctic Ocean primary production from 1980-2015: Implications of biogeochemical model parameterizations*. Sidney, BC: Fisheries and Oceans Canada, Science Branch, Pacific Region, Institute of Ocean Sciences. (Canadian Technical Report of Fisheries and Aquatic Sciences 3561).

Steiner, N, **Denman, K**, **McFarlane, N**, **Solheim, L.** 2006. Simulating the coupling between atmosphere–ocean processes and the planktonic ecosystem during SERIES. *Deep Sea Research Part II: Topical Studies in Oceanography* **53**(20–22): 2434–2454. DOI: http://dx.doi.org/10.1016/j.dsr2.2006.05.030.

Steiner, NS, **Reader, MC.** 2024. Trends and projections in climate-related stressors impacting Arctic marine ecosystems – A CMIP6 model analysis. *Journal of Geophysical Research: Oceans* **129**(11): e2024JC020970. DOI: http://dx.doi.org/10.22541/essoar.170680227.79348011/v1.

Steiner, NS, **Robert, M**, **Arychuk, M**, **Levasseur, ML**, **Merzouk, A**, **Peña, MA**, **Richardson, WA**, **Tortell, PD.** 2012. Evaluating DMS measurements and model results in the Northeast subarctic Pacific from 1996–2010. *Biogeochemistry* **110**(1): 269–285. DOI: http://dx.doi.org/10.1007/s10533-011-9669-9.

Timmermans, ML, **Marshall, J.** 2020. Understanding Arctic Ocean circulation: A review of ocean dynamics in a changing climate. *Journal of Geophysical Research: Oceans* **125**(4): e2018JC014378. DOI: http://dx.doi.org/10.1029/2018JC014378.

Toole, DA, **Slezak, D**, **Kiene, RP**, **Kieber, DJ**, **Siegel, DA.** 2006. Effects of solar radiation on dimethylsulfide cycling in the western Atlantic Ocean. *Deep Sea Research Part I: Oceanographic Research Papers* **53**(1): 136–153. DOI: http://dx.doi.org/10.1016/j.dsr.2005.09.003.

Trevena, A, **Jones, G.** 2012. DMS flux over the Antarctic sea ice zone. *Marine Chemistry* **134–135**: 47–58. DOI: http://dx.doi.org/10.1016/j.marchem.2012.03.001.

Vallina, SM, **Simó, R.** 2007. Strong relationship between DMS and the solar radiation dose over the global surface ocean. *Science* **315**(5811): 506–508. DOI: http://dx.doi.org/10.1126/science.1133680.

van Vuuren, DP, **Edmonds, J**, **Kainuma, M**, **Riahi, K**, **Thomson, A**, **Hibbard, K**, **Hurtt, GC**, **Kram, T**, **Krey, V**, **Lamarque, J-F**, **Masui, T**, **Meinshausen, M**, **Nakicenovic, N**, **Smith, SJ**, **Rose, SK.** 2011. The representative concentration pathways: An overview. *Climatic Change* **109**(1): 5–31. DOI: http://dx.doi.org/10.1007/s10584-011-0148-z.

Vancoppenolle, M, **Bopp, L**, **Madec, G**, **Dunne, J**, **Ilyina, T**, **Halloran, PR**, **Steiner, N.** 2013. Future Arctic

Ocean primary productivity from CMIP5 simulations: Uncertain outcome, but consistent mechanisms. *Global Biogeochemical Cycles* **27**(3): 605–619.

Wang, W-L, **Song, G**, **Primeau, F**, **Saltzman, ES**, **Bell, TG**, **Moore, JK.** 2020. Global ocean dimethyl sulfide climatology estimated from observations and an artificial neural network. *Biogeosciences* **17**(21): 5335–5354. DOI: http://dx.doi.org/10.5194/bg-17-5335-2020.

Webb, AL, **van Leeuwe, MA**, **den Os, D**, **Meredith, MP**, **Venables, HJ**, **Stefels, J.** 2019. Extreme spikes in DMS flux double estimates of biogenic sulfur export from the Antarctic coastal zone to the atmosphere. *Scientific Reports* **9**(1): 2233. DOI: http://dx.doi.org/10.1038/s41598-019-38714-4.

Willis, MD, **Leaitch, WR**, **Abbatt, JPD.** 2018. Processes controlling the composition and abundance of arctic aerosol. *Reviews of Geophysics* **56**(4): 621–671. DOI: http://dx.doi.org/10.1029/2018RG000602.

Wohl, C, **Villamayor, J**, **Galí, M**, **Mahajan, AS**, **Fernández, RP**, **Cuevas, CA**, **Bossolasco, A**, **Li, Q**, **Kettle, AJ**, **Williams, T**, **Sarda-Esteve, R**, **Gros, V**, **Simó, R**, **Saiz-Lopez, A.** 2024. Marine emissions of methanethiol increase aerosol cooling in the Southern Ocean. *Science Advances* **10**(48): eadq2465. DOI: http://dx.doi.org/10.1126/sciadv.adq2465.

Yang, GP, **Liu, XT**, **Li, L**, **Zhang, ZB.** 1999. Biogeochemistry of dimethylsulfide in the South China Sea. *Journal of Marine Research* **57**(1).

Yang, M, **Archer, SD**, **Blomquist, BW**, **Ho, DT**, **Lance, VP**, **Torres, RJ.** 2013. Lagrangian evolution of DMS during the Southern Ocean gas exchange experiment: The effects of vertical mixing and biological community shift. *Journal of Geophysical Research: Oceans* **118**(12): 6774–6790. DOI: http://dx.doi.org/10.1002/2013JC009329.

Zavarsky, A, **Goddijn-Murphy, L**, **Steinhoff, T**, **Marandino, CA.** 2018. Bubble-mediated gas transfer and gas transfer suppression of DMS and CO_2. *Journal of Geophysical Research: Atmospheres* **123**(12): 6624–6647. DOI: http://dx.doi.org/10.1029/2017JD028071.

How to cite this article: Haddon, A, Monahan, AH, Sou, T, Steiner, N. 2025. Simulated increases of future Arctic dimethylsulfide ocean concentrations, emissions and high-flux events. *Elementa: Science of the Anthropocene* 13(1). DOI: https://doi.org/10.1525/elementa.2024.00090

Domain Editor-in-Chief: Jody W. Deming, University of Washington, Seattle, WA, USA

Associate Editor: Mathieu Ardyna, Takuvik International Research Laboratory, CNRS/Université Laval, Québec City, Canada

Knowledge Domain: Ocean Science

Part of an Elementa Special Feature: Coupling of Ocean-Ice-Atmosphere Processes: From Sea-Ice Biogeochemistry to Aerosols and Clouds (CIce2Clouds)

Published: November 10, 2025 **Accepted:** August 12, 2025 **Submitted:** December 04, 2024

ELEMENTA Science of the Anthropocene

Elem Sci Anth is a peer-reviewed open access journal published by University of California Press.

OPEN ACCESS